Lund University

Thesis submitted for degree of Master of Science

Project Duration: 60 hp

Fall 2021

---

# Green's Functions Investigations in Quantum Transport Geometries

---

Author:
Philip Johansson

Supervisor:
Claudio Verdozzi


Lund University

Department of Physics

Division of Mathematical Physics

# Abstract

In this thesis we employ the non-equilibrium Green's function (NEGF) method to study both finite and infinite systems. We develop a codebase capable of computing the steady state interacting NEGF in open systems, i.e. tight-binding leads contacting a central region, in both Hartree-Fock (HF) and second Born (2B) approximations of particle-particle interactions. Furthermore, we use the exact interacting Green's function on finite regions to assess a method we found to compute any pair-correlation function. The method utilizes the Hellman-Feynman theorem applied to the Galitskii-Migdal formula for the total energy of a system. We find that it works well for finite systems, with and without currents, whereas for open (infinite) systems the method requires more care. Lastly, we briefly investigate a non-perturbative G1-G2 scheme; whether computing the two-particle Green's function in a subsystem approximates the full two-particle Green's function well. We find that the considered G1-G2 scheme provides results of variable accuracy, suggesting that our investigation is not exhaustive, and that the roles of system geometry and particle density should be further assessed.

# Acknowledgments

Firstly, I'd like to thank my supervisor Claudio Verdozzi, whose guidance and scientific insight has been invaluable. His motivation and determination inspires me to work harder. At this point, he is well aware of my fondness of the combination of programming and physics; this project has been the best of both worlds and for this I am very grateful.

Secondly, I recognize the interesting and valuable discussions had with P. Potts, P. Samuelsson, and D. Karlsson.

Lastly, I thank my friends and family for the encouragement and emotional support, both of which were greatly appreciated especially during these difficult times.

# Abbreviations

**ED** Exact Diagonalization
**EM** ElectroMagnetic
**DFT** Density Function Theory
**DMFT** Dynamical Mean Field Theory
**NEGF** Non-equilibrium Green's Function
**WBL** Wide-Band Limit
**HF** Hartree-Fock
**2B** Second Born
**FFTW** the Fastest Fourier Transform in the West
**GM** Galitskii-Migdal

# Contents

# Chapter 1

# Introduction and Motivation

Non-equilibrium quantum dynamics has recently become the subject of vast interest [1], largely due to great strides in experimental realizations of nanoscale devices utilizing quantum effects and experimental tools able to probe dynamics on short time scales [2]. Modern integrated circuits are susceptible to strong correlations and quantum effects, and their nature implies that they stay out-of-equilibrium when driven by an electrical bias. For example, modern day transistors that are on the scale of nanometers are small enough for the probability of quantum tunneling to be non-negligible and as such crucial components such as different types of memory can potentially leak charge and corrupt the information they hold. Studying the geometry and dynamics of such devices is useful in order to develop devices that can better withstand the unwanted effects of quantum mechanics. At the same time, with a better understanding of the quantum mechanical effects one might imagine that the effects could be exploited in new technological applications that were previously not possible.

Out-of-equilibrium many-body systems are vastly more complex than their equilibrium counterpart in that the possibilities are endless for how a system responds to a perturbation. Practically all real systems are both connected to an open environment and out of equilibrium.

Furthermore, out-of-equilibrium effects can result in exotic materials exhibiting strange phenomena and effects, see e.g. [3–5]. Other well-known phenomena include superconductivity [6] and ultra-cold atoms forming droplets [7]. Not only is this useful from purely scientific exploration perspective; rather, it can have a significant impact on technology, as in the case of superconductivity [8].

On a fundamental level, these exotic phenomena are the result of quan-

tum correlations, that is the quantum extension of the concept of correlation that stems from statistics. Specifically, in quantum mechanics this effect is most often referred to as quantum entanglement. It has its own name because correlations as predicted, and confirmed [9–11], by quantum mechanics are very different from correlations in classical physics.

The consequences of quantum entanglement (or just entanglement) on information theory have stimulated the emergence of a specific field of physics called *quantum information theory* [12]. The field is dedicated to studying how information is contained in quantum systems and how quantum information can be manipulated to form quantum computing circuits. This has resulted in new ways to encrypt and communicate information and even provides a method by which information can be teleported [12]. The exotic behavior of non-equilibrium systems is now accessible by experiments allowing for theoretical models and tools to be tested. Furthermore, strong correlations can be probed and manipulated with ultra-fast lasers [13, 14] allowing for experimental realizations of simple quantum computers [15]. The complementarity of experiments and theory ultimately rewards us with greater understanding and better technology.

Naturally, describing nano systems and their dynamics requires a quantum mechanical description. Typically, physical systems are much too complicated and/or large which makes first principles treatments very difficult (if not impossible), and as such theoreticians often refer to model systems to simplify the description. Although a simplified description, model systems can still capture much of the exciting physics of real materials. The starting point in quantum mechanics is the Hamiltonian, the operator fully describing the system. If the system is "small" enough (which seldom is the case), one can simply diagonalize the Hamiltonian and gain the full knowledge of the systems eigenstates. If the system is initially in its ground state it will remain there so long as it is not perturbed, and nothing extraordinarily interesting (by today's standards) occurs. This approach is called Exact Diagonalization (ED) and can even be applied to systems driven out of equilibrium by thermal/electrical bias or by interacting directly with an EM-field, again provided the system is small. Generally this approach scales poorly with system size and as such is typically used for small isolated systems, but since the method is exact, it provides a natural benchmark for other methods.

Open systems belong to a different category altogether; they typically consist of a nanostructure connected to an environment. The latter is usually very large or in fact (for mathematical convenience) infinite. In this

case, appropriate methods include Density functional Theory (DFT) [16], Dynamical Mean Field Theory (DFMT) [17] and correlator based methods. Common among these methods is that one works with some other quantity rather than the many-body wave function as in ED. This typically results in more favorable scaling with system size despite still allowing one to compute the observable of interest. Another powerful tool of this class, and of central importance to this thesis, is the Green's Function [18].

There are a few flavors of Green's function formalism; the zero-temperature, finite temperature and non-equilibrium Green's function (NEGF), with the latter being the more general of the three. The NEGF method is a very appropriate tool for studying transport geometries. A generic quantum transport system consists of some finite system, the device system (e.g. a molecule), attached to leads (e.g. wires) acting as baths with which the device system can exchange particles and heat, see figure 1.1.

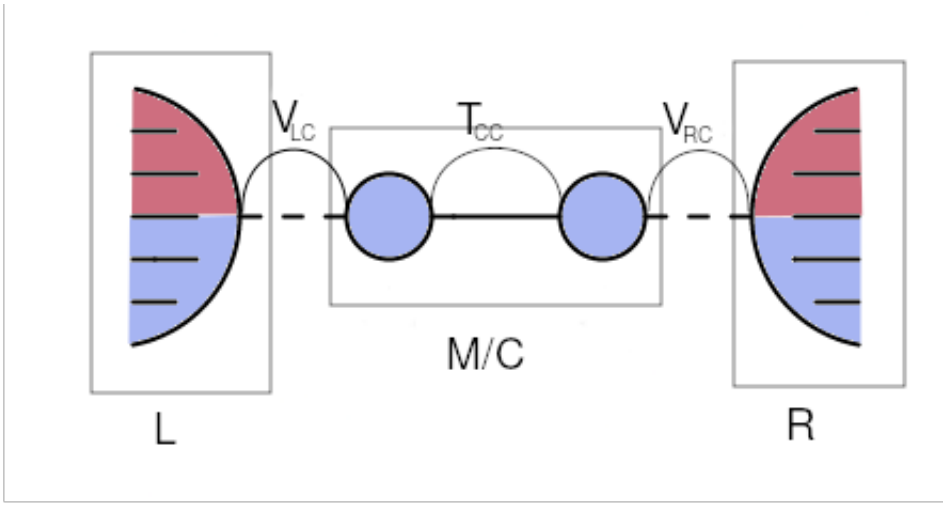


Figure 1.1: Depiction of generic transport system.
"L": Left lead, "M/C": Molecule/Center, "R": Right lead
"$V_{LC}$": Hopping from L to M/C, "$V_{RC}$": Hopping from R to M/C
"$T_{CC}$": Hopping between sites in Molecule/Center.

By applying a voltage bias over the device system, one can generate a current through it and study the non-equilibrium dynamics of the device system, typically associated with open systems, and can perturbatively include Coulomb interactions.

Furthermore, in the steady state regime, it is possible to have a descrip-

tion in frequency space, as opposed to the time-domain. Despite not being time-dependent, the system can be subject to electrical and thermal biases, however the dynamics of the transient region is lost.

This work will build upon previous research [19], where a chain of two coupled dots connected to one-dimensional non-interacting leads was studied. Said work aimed to study the interdot entanglement as a result of thermal and chemical biases, and within a fully analytical approach. In order to keep the approach entirely analytical, some approximations had to be introduced in the treatment, such as considering only non-interacting quantum dots, using the wide-band limit (WBL), and assuming the Fermi-Dirac distribution to be constant in the region of interest. We instead employ a numerical approach, which allows us to discard the aforementioned approximations as well as also treat electron-electron interactions.

The drastic effects that can arise from correlations necessitate an accurate description of the Coulomb interaction in theoretical models. In the Green's functions method, one defines a so-called self-energy which contains the effect of the interactions between particles. Typically, it is much too difficult (or even impossible) to calculate the self-energy exactly and one has to resort to approximating it. From a theoretical point of view, the self-energy approximation in terms of Feynman diagrams, provides a convenient perturbative expansion of the self-energy, however the aforementioned perturbative nature does not provide a complete description, see e.g. [20].

An important problem in current research with NEGF (and even with Green's functions in equilibrium) is how to deal with strong correlations.

In an attempt to study correlations in a transport geometry such as the one described above, via concurrence [21], we developed the skeleton of a new method for computing correlation functions (see Sec. 6.1.2). The method utilizes the Hellman-Feynman theorem applied to the Galitskii-Migdal formula for the total energy. The method was then tested on both infinite and finite systems (see Sec. 6.2.2).

Finally, we performed a very preliminary investigation into a possible new route around the partial sum approximation for diagrams. We investigate whether the self-energy can be computed directly from a two-particle Green's function of a finite system and adjusted to match the original system. In this way, the method is no longer perturbative. When computing the self-energy perturbatively, one needs to choose what diagrams to include. This means that the approximation used only works well for a small set of systems and parameters, thus the approximation must be chosen appropriately. This significant drawback, would be eliminated with a non-perturbative technique

such as this two-particle Green's function approach preliminarily explored here.

# Chapter 2

# Theoretical Background A

## 2.1 Time Evolution

The Shrödinger equation is the fundamental equation of motion in non-relativistic quantum mechanics:

$$i\hbar \frac{\mathrm{d}}{\mathrm{dt}} |\Psi(t)\rangle = \hat{H}(t) |\Psi(t)\rangle , \tag{2.1}$$

where $\hat{H}$ is the Hamiltonian corresponding to the system in question. Provided the Hamiltonian is time-independent, i.e. $\hat{H}(t) = \hat{H}$, equation 2.1 is straightforwardly solved by:

$$|\Psi(t)\rangle = e^{-i\hat{H}(t-t_0)/\hbar} |\Psi(t_0)\rangle . \tag{2.2}$$

Solving this numerically by inserting a complete set of eigenstates of $\hat{H}$ is known as Exact Diagonalization (ED) [22], and can in principle provide the exact solution to any time-independent problem. However, in practice this involves diagonalizing the Hamiltonian in a basis of the Hilbert space whose dimension scales exponentially with system size. Thus, ED is more suitable for small systems where the cardinality of the Hilbert space is manageable.

For time-dependent Hamiltonians, the integrating factor that solves the differential equation in 2.1 becomes more general and is referred to as the time-evolution operator [23]:

$$\hat{U}(t, t_0) = T \left\{ e^{-i \int_{t_0}^{t} dt' \hat{H}(t')} \right\} , \tag{2.3}$$

where the time-evolution operator in equation 2.2 is a particular case when $\hat{H}(t) \equiv \hat{H}$. Here, $T$ is the time ordering operator which orders the time

arguments chronologically.

Then, in general, the solution to the Shrödinger equation is given by:

$$|\Psi(t)\rangle = \hat{U}(t, t_0) \, |\Psi(t_0)\rangle \, . \tag{2.4}$$

With the time-dependent wave function we can compute time-dependent expectation values:

$$O(t) = \langle \Psi(t)| \, \hat{O} \, |\Psi(t)\rangle = \langle \Psi(t_0)| \, \hat{U}(t_0, t) \hat{O} \hat{U}(t, t_0) \, |\Psi(t_0)\rangle \, . \tag{2.5}$$

This brings us to the definition of the Heisenberg operator, where in equation 2.5 one lets the evolution operators act on the operator transferring the time-dependence, from the wave function, to it:

$$\hat{O}_H(t) = \hat{U}(t_0, t) \hat{O} \hat{U}(t, t_0). \tag{2.6}$$

Furthermore, in a grand canonical ensemble the expectation value is calculated as:

$$\langle \hat{O}_H(t) \rangle = \mathrm{Tr} \left\{ \hat{\rho} \hat{O}_H(t) \right\}, \tag{2.7}$$

where $\hat{\rho}$ is the density matrix:

$$\hat{\rho} = \frac{e^{-\beta(\hat{H} - \mu \hat{N})}}{\mathrm{Tr} \left\{ e^{-\beta(\hat{H} - \mu \hat{N})} \right\}}. \tag{2.8}$$

## 2.2 Exact Diagonalization (ED)

Exact diagonalization is the method of exactly finding the eigenstates and energies of the relevant Hamiltonian. This makes it a very powerful method in that it is exact, however much of the information obtained is superfluous and as such much of the effort is wasted.

We start from the time-evolved wave function:

$$|\Psi(t)\rangle = \hat{U}(t, t_0) \, |\Psi(t_0)\rangle \, . \tag{2.9}$$

The initial state is chosen by the user and can be taken to be either the ground state of the system before some perturbation, or a specific state. If the initial state is an eigenstate of a time-independent Hamiltonian, the evolution of the initial state amounts to a phase shift:

$$|\Psi(t)\rangle = e^{-i\hat{H}(t - t_0)} \, |\Psi(t_0)\rangle = e^{-iE_0(t - t_0)} \, |\Psi(t_0)\rangle \, . \tag{2.10}$$

Conversely, for an arbitrary initial state, that is not an eigenstate of the Hamiltonian, the system exhibits dynamics:

$$|\Psi(t)\rangle = e^{-i\hat{H}(t-t_0)}\,|\Psi(t_0)\rangle = \sum_\lambda e^{-iE_\lambda(t-t_0)}\,|\lambda\rangle\,\langle\lambda|\Psi(t_0)\rangle$$
$$= \sum_\lambda c_\lambda e^{-iE_\lambda(t-t_0)}\,|\lambda\rangle\,. \tag{2.11}$$

The set of eigenvectors of the Hamiltonian $\{|\lambda\rangle\}$ spans the Hilbert space and so the initial state can in principle evolve into any conceivable state.

For a time-dependent Hamiltonian, a numerical approach is further complicated:

$$|\Psi(t)\rangle = \hat{U}(t,t_0)\,|\Psi(t_0)\rangle = e^{-i\int_{t_0}^{t} dt'\hat{H}(t')}\,|\Psi(t_0)\rangle\,. \tag{2.12}$$

In equation 2.12 the integral can be decomposed into its Riemann sum with the midpoint rule:

$$e^{-i\int_{t_0}^{t} dt'\hat{H}(t')}\,|\Psi(t_0)\rangle \approx \prod_{k=1}^{N} e^{-i\hat{H}(t_0+k\Delta t)\Delta t}\,|\Psi(t_0)\rangle\,. \tag{2.13}$$

The Hamiltonian will then need to be diagonalized on every time-step $(t_0 + k\Delta t)$.

To see the downfall of this method, consider the studying a system of 50 one-particle states, occupied by 4 electrons (2 spin-up and 2 spin-down). The size of the Hamiltonian is then $\binom{50}{2}^2 = 1500625$. Furthermore, say the system is time-dependent, then the numerical solution is obtained after diagonalizing a $1500625 \times 1500625$ matrix, (often) thousands of times.[1]

[1] For a more detailed study using ED see e.g. [24]

## 2.3 Keldysh Contour

The exponential in the density matrix $e^{-\beta \hat{H}_0}$ can be interpreted as an imaginary-time time evolution so that we can write the expectation value:

$$\langle \hat{O}_H(t) \rangle = \frac{\mathrm{Tr}\left\{ \hat{U}(t_0 - i\beta, t_0)\hat{U}(t_0, t)\hat{O}\hat{U}(t, t_0) \right\}}{\mathrm{Tr}\{\hat{U}t_0 - i\beta, t_0)\}}. \tag{2.14}$$

This interpretation allows for an extension of the real-time evolution to the complex plane, specifically the expression in the numerator of equation 2.14 follows the path in figure 2.1.

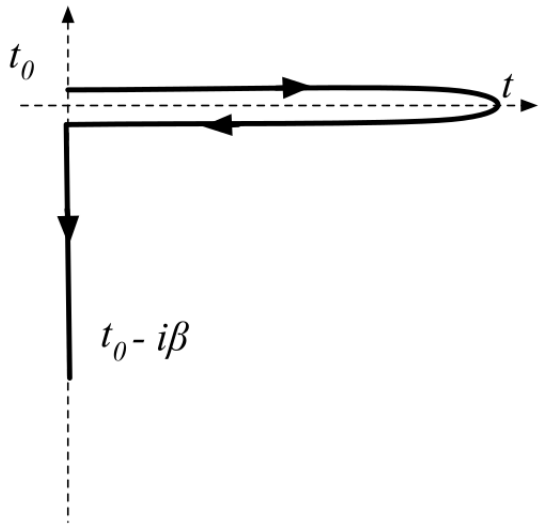


Figure 2.1: $t$-dependent time contour.

We can extend the contour, so that its length is no longer dependent on $t$:

$$\langle \hat{O}_H(t) \rangle = \frac{\mathrm{Tr}\left\{ \hat{U}(t_0 - i\beta, t_0)\hat{U}(t_0, t)\hat{O}\hat{U}(t, \infty)\hat{U}(\infty, t_0) \right\}}{\mathrm{Tr}\{\hat{U}\{t_0 - i\beta, t_0)\}}, \tag{2.15}$$

where now the expression follows the contour in figure 2.2

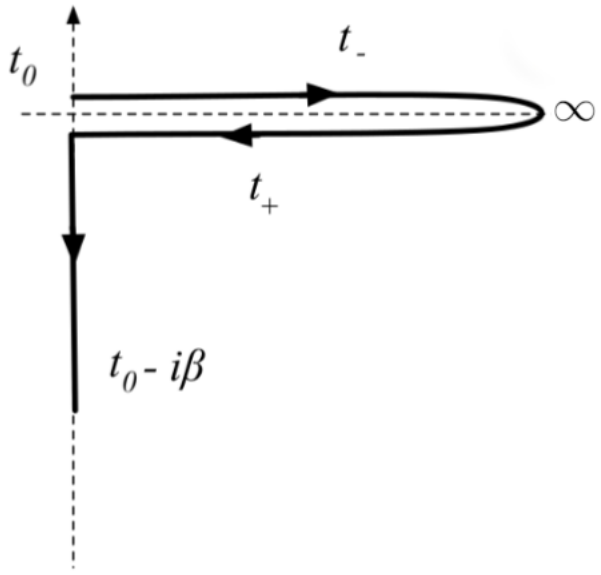


Figure 2.2: The Keldysh contour.

The extended contour in figure 2.2 is the Keldysh contour [25]. We define the forward branch to be the track from $t_0$ to $\infty$, and the backward branch the track from $\infty$ to $t_0$. We denote times on the forward (backward) branch by $t_-(t_+)$ [26]. We can then write the expectation value in equation 2.15 in a more compact way:

$$O(z) = \frac{\mathrm{Tr}\left[\mathcal{T}\left\{e^{-i\int_\gamma d\bar{z}\ \hat{H}(\bar{z})}\hat{O}(\bar{z})\right\}\right]}{\mathrm{Tr}\left[\mathcal{T}\left\{e^{-i\int_\gamma d\bar{z}\ \hat{H}(\bar{z})}\right\}\right]}. \tag{2.16}$$

The $\int_\gamma$ in equation 2.16 means that $\bar{z}$ takes values on the contour in figure 2.2, where now $\bar{z} \in \mathbb{C}$, and $\mathcal{T}$ orders its arguments in chronological order:

$$\mathcal{T}a(t)b(t') = \begin{cases} a(t)b(t'),\ t > t' \\ b(t')a(t),\ t < t'. \end{cases} \tag{2.17}$$

Note that times on the forward branch ($t_-$) are always earlier than times on the backward branch($t_+$).

### 2.3.1 Langreth Rules

As we will see, in the NEGF formalism we utilize the Keldysh contour in order to compactify the description, and in the formalism we find expressions that involve convolutions or products of functions on the contour. In order to work with these expressions either analytically or numerically we need to convert them to real-time. This is the purpose of this section, and of Langreth rules [27], namely to determine identities that convert functions with arguments on the contour to functions with real-time arguments. We will focus on two-point operator correlators since they are the ones that make up the one-particle Green's function, however, the identities can be derived for more general $n$-point correlators, see, e.g., [28].

We can define a template for a Keldysh function, i.e. a function with arguments on the Keldysh contour:

$$k(z, z') = k^{\delta}(z)\delta(z, z') + \theta(z, z')k^{>}(z, z') + \theta(z', z)k^{<}(z, z'), \tag{2.18}$$

where $\delta(z - z')$ is the delta function and $\theta(z, z')$ is the heaviside function. In equation 2.18, $k^{\delta}$ satisfies $k^{\delta}(t_+) = k^{\delta}(t_-)$ with $t_-$ lying on the forward branch and $t_+$ on the backwards, in figure 2.2. The superscripts $< / >$ (lesser/greater) indicate the relationship between the arguments.

As we saw when constructing the contour, the vertical axis contains physical information as well, hence in order to extract that from $k(z, z')$ we need all combinations of arguments on the contour and their definition in terms of real-time arguments.

We define the lesser/greater Keldysh components with both arguments belonging to the real-time axis:

$$k^{<}(t, t') = k(t_-, t'_+) \tag{2.19}$$

$$k^{>}(t, t') = k(t_+, t'_-). \tag{2.20}$$

We also define the Keldysh components with one real-time argument and one imaginary-time:

$$k^{\lceil}(\tau, t) = k(t_0 - i\tau, t_\pm) \tag{2.21}$$

$$k^{\rceil}(t, \tau) = k(t_\pm, t_0 - i\tau), \tag{2.22}$$

where the symbols $\lceil / \rceil$ refers to the relative positions of the arguments, left indicating the first argument is imaginary and right the second. Finally, the Keldysh component with arguments that both lie on the imaginary, or vertical, axis:

$$k^{M}(\tau, \tau') = k(t_0 - i\tau, t_0 - i\tau'). \tag{2.23}$$

Equipped with the different Keldysh components of $k(z, z')$, we now turn to more combinations of Keldysh functions and how to decompose them into their constituents' Keldysh components. Consider, e.g., the convolution of two Keldysh functions:

$$c(z, z') = \int_\gamma d\bar{z}\ a(z, \bar{z})b(\bar{z}, z'), \tag{2.24}$$

where the subscript $\gamma$ indicates the integral variable $\bar{z}$ takes values on the contour.

Let us start with the lesser component of $c(z, z')$. Expanding $a(z, \bar{z})$ and $b(\bar{z}, z')$ into their templates:

$$\begin{aligned} c^<(t, t') = c(t_-, t'_+) = a^\delta(t_-)b(t_-, t'_+) + a(t_-, t'_+)b^\delta(t'_+) + \\ \int_\gamma d\bar{z}\ \big[\theta(t_-, \bar{z})\theta(t'_+, \bar{z})a^>(t_-, \bar{z})b^<(\bar{z}, t'_+) + \\ + \theta(\bar{z}, t_-)\theta(\bar{z}, t'_+)a^<(t_-, \bar{z})b^>(\bar{z}, t'_+) + \\ + \theta(t'_+, \bar{z})\theta(\bar{z}, t_-)a^<(t_-, \bar{z})b^<(\bar{z}, t'_+)\big], \end{aligned} \tag{2.25}$$

where the terms that are prefixed by something equivalent to $\theta(z, z')$ are removed since they belong to the greater component of $c(z, z')$.

In equation 2.25 we can utilize the Heaviside functions to write the integrals with explicit limits:

$$\begin{aligned} c^<(t, t') = a^\delta(t)b^<(t, t') + a^<(t, t')b^\delta(t') + \\ \int_{t_{0-}}^{t_-} d\bar{z}\ a^>(t_-, \bar{z})b^<(\bar{z}, t'_+) + \int_{t_-}^{t'_+} d\bar{z}\ a^<(t_-, \bar{z})b^<(\bar{z}, t'_+) + \\ + \int_{t'_+}^{t_0 - i\beta} d\bar{z}\ a^<(t_-, \bar{z})b^>(\bar{z}, t'_+). \end{aligned} \tag{2.26}$$

We can then cast equation 2.26 onto a real-time axis and an imaginary-time axis separately:

$$c^<(t,t') = a^\delta(t)b^<(t,t') + a^<(t,t')b^\delta(t') + \int_{t_0}^{t} d\bar{t}\; a^>(t,\bar{t})b^<(\bar{t},t') + \\ + \int_{t}^{t'} d\bar{t}\; a^<(t,\bar{t})b^<(\bar{t},t') + \int_{t'}^{t_0} d\bar{t}\; a^<(t,\bar{t})b^>(\bar{t},t') + \\ -i\int_0^\beta d\bar{\tau}\; a^\rceil(t,\bar{\tau})b^\lceil(\bar{\tau},t'). \tag{2.27}$$

We can split the first integral in the second line, $\int_t^{t'} = \int_t^{t_0} + \int_{t_0}^{t'}$:

$$c^<(t,t') = a^\delta(t)b^<(t,t') + a^<(t,t')b^\delta(t') + \\ + \int_{t_0}^{t} d\bar{t}\; [a^>(t,\bar{t}) - a^<(t,\bar{t})]b^<(\bar{t},t') - \int_{t_0}^{t'} d\bar{t}\; a^<(t,\bar{t})[b^>(\bar{t},t') - b^<(\bar{t},t')] \\ -i\int_0^\beta d\bar{\tau}\; a^\rceil(t,\bar{\tau})b^\lceil(\bar{\tau},t'). \tag{2.28}$$

At this point it is convenient to define two new Keldysh components:

$$k^R(t,t') = k^\delta(t)\delta(t,t') + \theta(t,t')[k^>(t,t') - k^<(t,t')] \tag{2.29}$$
$$k^A(t,t') = k^\delta(t)\delta(t,t') - \theta(t',t)[k^>(t,t') - k^<(t,t')], \tag{2.30}$$

with which we can rewrite the lesser component of $c(z,z')$ as:

$$c^<(t,t') = \int_{t_0}^{\infty} d\bar{t}[a^<(t,\bar{t})b^A(\bar{t},t') + a^R(t,\bar{t})b^<(\bar{t},t')] \\ - i\int_0^\beta d\bar{\tau} a^\rceil(t,\bar{\tau})b^\lceil(\bar{\tau},t'). \tag{2.31}$$

We can compactify it by using shorthand notations for convolutions on the real-time axis and imaginary-time axis respectively:

$$f\cdot g = \int_{t_0}^{\infty} d\bar{t} f(\bar{t})g(\bar{t})$$
$$f\star g = -i\int_0^\beta d\bar{\tau} f(\bar{\tau})g(\bar{\tau}).$$

With this notation, the lesser component of $c(z, z')$ can be written as:

$$c^< = a^< \cdot b^A + a^R \cdot b^< + a^\rceil \star b^\lceil. \tag{2.32}$$

In a very similar manner, the greater component can be found to be:

$$c^> = a^> \cdot b^A + a^R \cdot b^> + a^\rceil \star b^\lceil. \tag{2.33}$$

From the lesser and greater decomposition, the retarded and advanced can be obtained. The left/right and Matsubara components can be found by the same logic used to determine the lesser/greater.

It is worth noting that to obtain the Langreth rules in the frequency domain, we simply take an identity in the time-domain and Fourier transform it. To see how to Fourier transform convolutions, consider the convolution in the long-time limit:

$$c(t - t') = \int_{t_0}^{\infty} d\bar{t}\ a(t - \bar{t})b(\bar{t} - t') \Leftrightarrow c(t) = \int_{-\infty}^{t-t_0} d\bar{t}\ a(t)b(t - \bar{(t)}), \tag{2.34}$$

which in the limit $t \to \infty$ becomes:

$$c(t) = \int_{-\infty}^{\infty} d\bar{t}\ a(t)b(t - \bar{t}). \tag{2.35}$$

Equation 2.35 describes a typical convolution for which the Fourier transform is known:

$$c(\omega) = a(\omega)b(\omega). \tag{2.36}$$

## 2.4 Green's functions

Equipped with the notion of the Keldysh contour and the Langreth rules, we are ready to define the one-particle non-equilibrium Green's function in a grand canonical ensemble:

$$G(1,2) \equiv -i \left\langle \mathcal{T}\{\hat{\psi}(1)\hat{\psi}^\dagger(2)\}\right\rangle = -i\frac{\mathrm{Tr}\left[\mathcal{T}\left\{e^{-i\int_\gamma d\bar{z}\ \hat{H}(\bar{z})}\hat{\psi}(1)\hat{\psi}^\dagger(2)\right\}\right]}{\mathrm{Tr}\left[\mathcal{T}\left\{e^{-i\int_\gamma d\bar{z}\ \hat{H}(\bar{z})}\right\}\right]}, \quad (2.37)$$

where the arguments $(1,2)$ are shorthand notation for $(x_1\sigma_1; z_1,\ x_2\sigma_2; z_2)$ [26]. The power of the contour becomes apparent here; by discarding all but the imaginary track of the contour the NEGF formalism reduces to the Matsubara formalism, by extending the contour to the left in figure 2.2 and including the equilibrium Hamiltonian up until $t_0$ an adiabatic switching off the interaction can be treated and of course the exact non-equilibrium Green's function on the contour in figure 2.2 can be calculated. That is to say, this definition of the Green's function contains all other flavors [26].

To acquire some intuition for the Green's function we can expand the time-ordering [29]:

$$G(1,2) = \theta(t_1 - t_2)G^>(1,2) + \theta(t_2 - t_1)G^<(1,2). \quad (2.38)$$

As we saw in section 2.3, $G(1,2)$ meets the requirements for a Keldysh function with $G^\delta = 0$. From the definition of greater/lesser, we can write:

$$G^>(1,2) = G(x_1t_{1+}, x_2t_{2-}) = -i\left\langle\hat{\psi}(1)\hat{\psi}^\dagger(2)\right\rangle \quad (2.39)$$

$$G^<(1,2) = G(x_1t_{1-}, x_2t_{2+}) = i\left\langle\hat{\psi}^\dagger(2)\hat{\psi}(1)\right\rangle. \quad (2.40)$$

Here we can see that the greater Green's function, in equation 2.39, is the correlation function corresponding to injecting a particle at position $x_2$ with spin $\sigma_2$ at time $z_2$ and removing it at $x_1\sigma_1; z_1$ [29]. Similarly, the lesser Green's function describes the propagation of a hole. Furthermore, at equal times the lesser Green's function is exactly the one-particle density matrix, bar the $i$. It is precisely from this that one can calculate observables since a general one particle expectation value has the form:

$$\begin{aligned}\langle \hat{O}(x_1, x_2; t)\rangle &= \int dx_1 dx_2 \ \langle \hat{\psi}^\dagger(x_1 t) \langle x_1 | \hat{O}(t) | x_2 \rangle \hat{\psi}(x_2 t)\rangle = \\ &= -i \int dx_1 dx_2 \ O(x_1, x_2; t) G^<(x_1 t, x_2 t).\end{aligned} \tag{2.41}$$

### 2.4.1 Equation of Motion for $G$

The one-particle Green's function consists of time-ordered field operators in the Heisenberg picture, so it is natural to start with the Heisenberg equation of motion for the field operators $\hat{\psi}(1)$ and $\hat{\psi}^\dagger(2)$:

$$\partial_z \hat{\psi}(xz) = i[\hat{H}(z), \hat{\psi}(xz)] = i\hat{U}(t_{0-}, z)[\hat{H}, \hat{\psi}(x)]\hat{U}(z, t_{0-}) \tag{2.42}$$

$$\partial_{z'} \hat{\psi}^\dagger(x'z') = i[\hat{H}(z'), \hat{\psi}^\dagger(x'z')] = i\hat{U}(t_{0-}, z')[\hat{H}, \hat{\psi}^\dagger(x')]\hat{U}(z', t_{0-}). \tag{2.43}$$

The general type of Hamiltonian treated in this thesis can be written as:

$$\begin{aligned}\hat{H}(z) = &\int dx \ \hat{\psi}^\dagger(x) h_0(xz) \hat{\psi}(x) + \\ &+ \frac{1}{2} \int dx dx' \ v(x, x'; z) \hat{\psi}^\dagger(x) \hat{\psi}^\dagger(x') \hat{\psi}(x') \hat{\psi}(x).\end{aligned} \tag{2.44}$$

For the equation of motions of the field operators we need compute the commutator of the Hamiltonian with the respective field operator, in the Schrödinger picture:

$$\begin{aligned}[\hat{H}, \hat{\psi}(x)] = &\int dx' \ h_0(x')[\hat{\psi}^\dagger(x')\hat{\psi}(x'), \hat{\psi}(x)] + \\ &+ \frac{1}{2} \int dx' dx'' \ v(x', x'')[\hat{\psi}^\dagger(x')\hat{\psi}^\dagger(x'')\hat{\psi}(x'')\hat{\psi}(x'), \hat{\psi}(x)] = \\ &= -h_0(x)\hat{\psi}(x) - \int dx' v(x, x') \hat{\psi}^\dagger(x') \hat{\psi}(x') \hat{\psi}(x).\end{aligned} \tag{2.45}$$

The equation of motion of the annihilation operator then becomes:

$$\begin{aligned}i\partial_z \hat{\psi}(xz) = &h_0(xz)\hat{\psi}(xz) \\ &+ \int dx' dz' \ v(xz, x'z') \delta(z - z') \hat{\psi}^\dagger(x'z') \hat{\psi}(x'z') \hat{\psi}(xz).\end{aligned} \tag{2.46}$$

If we compare equation 2.46 to the derivative of the Green's function:

$$
\begin{aligned}
i\partial_z G(xz,x'z') &= \partial_z \langle \mathcal{T}\left[\hat{\psi}(xz)\hat{\psi}^\dagger(x'z')\right]\rangle = \\
&= \partial_z \left[\theta(z-z')\langle\hat{\psi}(xz)\hat{\psi}^\dagger(x'z')\rangle - \theta(z'-z)\langle\hat{\psi}^\dagger(x'z')\hat{\psi}(xz)\rangle\right] = \\
&= \delta(z-z')(\langle\hat{\psi}(xz)\hat{\psi}^\dagger(x'z')\rangle + \langle\hat{\psi}^\dagger(x'z')\hat{\psi}(xz)\rangle) + \\
&+\theta(z-z')\partial_z\langle\hat{\psi}(xz)\hat{\psi}^\dagger(x'z')\rangle - \theta(z'-z)\partial_z\langle\hat{\psi}^\dagger(x'z')\hat{\psi}(xz)\rangle = \\
&= \delta(z-z')\delta(x-x') + \\
&+\theta(z-z')\partial_z\langle\hat{\psi}(xz)\hat{\psi}^\dagger(x'z')\rangle - \theta(z'-z)\partial_z\langle\hat{\psi}^\dagger(x'z')\hat{\psi}(xz)\rangle .
\end{aligned}
\tag{2.47}
$$

By inspection, we can see that if we multiply equation 2.46 from the right with $-i\theta(z-z')\hat{\psi}^\dagger(x'z')$ and from the left with $i\theta(z'-z)\hat{\psi}^\dagger(x'z')$ respectively, and take their expectation values in the grand canonical ensemble we have exactly the two terms from equation 2.47.

$$
\begin{aligned}
i\partial_z G(xz,x'z') &= \delta(z-z')\delta(x-x') + h(xz)G(xz,x'z') + \\
&\int d\bar{x}d\bar{z}\; v(xz,\bar{x}\bar{z})\left[\theta(z-z')\langle\hat{\psi}^\dagger(\bar{x}\bar{z})\hat{\psi}(\bar{x}\bar{z})\hat{\psi}(xz)\hat{\psi}^\dagger(x'z')\rangle\right. \\
&\left. -\theta(z'-z)\langle\hat{\psi}^\dagger(x'z')\hat{\psi}^\dagger(\bar{x}\bar{z})\hat{\psi}(\bar{x}\bar{z})\hat{\psi}(xz)\rangle\right] = \\
&= \delta(z-z')\delta(x-x') + h(xz)G(xz,x'z') \\
&+ \int d\bar{x}d\bar{z}\; v(xz,\bar{x}\bar{z})G^{(2)}(xz,\bar{x}\bar{z};x'z',\bar{x}\bar{z}^+),
\end{aligned}
\tag{2.48}
$$

where we have defined the interaction to contain the delta function in time, i.e. it is time-local: $v(xz,\bar{x}\bar{z}) = v(x,\bar{x})\delta(z-z')$, and defined the two-particle Green's function as:

$$
G^{(2)}(1,2;3,4) = \frac{1}{i^2}\langle\mathcal{T}\hat{\psi}(1)\hat{\psi}(2)\hat{\psi}^\dagger(4)\hat{\psi}^\dagger(3)\rangle . \tag{2.49}
$$

Then we can write the equation of motion more compactly [26, 29]:

$$
\left[i\partial_z - h(1)\right]G(1,2) = \delta(1-2) + \int d3\; v(1,3)G^{(2)}(1,3;2,3^+). \tag{2.50}
$$

Here, the "+" sign in $3^+$ means that $z_3^+$ is infinitesimally later than $z_3$ and ensures the field operators are ordered correctly after the time-ordering.

The one-particle Green's function thus depends on the two-particle Green's function, in turn the two-particle Green's function depends on the three-particle Green's function and so on; this is the Martin-Schwinger hierarchy [26].

### 2.4.2 Lehmann Representation

The definition of the Green's function $G(1,2)$ in equation 2.37 makes no assumptions on the structure of the Hamiltonian. If, on the other hand, we restrict ourselves to time-independent Hamiltonians we can write the Green's function as:

$$iG(1,2) = \sum_k \rho_k \langle \Psi_k | \mathcal{T} \left\{ \hat{\psi}(1)\hat{\psi}^\dagger(2) \right\} | \Psi_k \rangle . \tag{2.51}$$

The operators in equation 2.51 are in the Heisenberg picture, so we can write out their evolution explicitly.

$$\begin{aligned} iG(x_1t_1, x_2t_2) = \sum_k \rho_k \Big[ \\ \theta(t_1-t_2) \langle \Psi_k | e^{i\hat{H}(t_1-t_0)} \hat{\psi}(x_1) e^{-i\hat{H}(t_1-t_2)} \hat{\psi}^\dagger(x_2) e^{-i\hat{H}(t_2-t_0)} | \Psi_k \rangle \\ -\theta(t_2-t_1) \langle \Psi_k | e^{i\hat{H}(t_2-t_0)} \hat{\psi}^\dagger(x_2) e^{-i\hat{H}(t_2-t_1)} \hat{\psi}(x_1) e^{-i\hat{H}(t_1-t_0)} | \Psi_k \rangle \Big] . \end{aligned} \tag{2.52}$$

We can insert a complete set of eigenstates of $\hat{H}$:

$$\begin{aligned} iG(x_1t, x_2t_2) = \sum_k \rho_k \sum_\lambda \Big[ \\ \theta(t_1-t_2) e^{iE_k(t_1-t_2)} \langle \Psi_k | \hat{\psi}(x_1) e^{-iE_\lambda(t_1-t_2)} | \lambda \rangle \langle \lambda | \hat{\psi}^\dagger(x_2) | \Psi_k \rangle \\ -\theta(t_2-t_1) e^{-iE_k(t_1-t_2)} \langle \Psi_k | \hat{\psi}^\dagger(x_2) e^{iE_\lambda(t_2-t_1)} | \lambda \rangle \langle \lambda | \hat{\psi}(x_1) | \Psi_k \rangle \Big] = \\ = \sum_{k\lambda} \rho_k \Big[ \\ \theta(t_1-t_2) e^{-i(E_\lambda-E_k)(t_1-t_2)} \langle \Psi_k | \hat{\psi}(x_1) | \lambda \rangle \langle \lambda | \hat{\psi}^\dagger(x_2) | \Psi_k \rangle \\ -\theta(t_2-t_1) e^{i(E_\lambda-E_k)(t_1-t_2)} \langle \Psi_k | \hat{\psi}^\dagger(x_2) | \lambda \rangle \langle \lambda | \hat{\psi}(x_1) | \Psi_k \rangle \Big] . \end{aligned} \tag{2.53}$$

Note here that in equation 2.53, if the states $|\Psi_k\rangle$ have $N$ particles, the states $|\lambda\rangle$ have $N+1$ in the second to last line and $N-1$ in the last line.

The Green's function now depends only on the time-difference $t = t_1 - t_2$, so we can Fourier transform it. We then have to compute:

$$\int_{-\infty}^{\infty} dt\ e^{i\omega t}\theta(\pm t)e^{\pm i(E_\lambda - E_k)t} = \int_{0}^{\infty} dt\ e^{i\omega t}\theta(\pm t)e^{\pm i(E_\lambda - E_k)t}. \tag{2.54}$$

The frequency representation of the Heaviside function is:

$$\theta(t - t') = i\int_{-\infty}^{\infty} \frac{e^{-i\omega(t-t')}}{w + i\delta}. \tag{2.55}$$

The integral in equation 2.55 is a contour integral over the complex plane. If we insert equation 2.55 into equation 2.54:

$$\int_0^\infty dt\ \int_{-\infty}^{\infty} \frac{dw'}{2\pi} \frac{e^{\mp i\omega' t} e^{i(\omega \pm (E_\lambda - E_k))}}{\omega' + i\delta} = \frac{i}{\omega \pm (E_\lambda - E_k) \mp i\delta}\ . \tag{2.56}$$

Then, the Green's function in the frequency domain can be written as:

$$G(x_1, x_2; \omega) = \sum_{k\lambda} \left[ \frac{\Phi_{k\lambda}(x_1)\Phi^*_{\lambda k}(x_2)}{\omega + (E_\lambda - E_k) - i\delta} + \frac{\Phi^*_{k\lambda}(x_2)\Phi_{\lambda k}(x_1)}{\omega - (E_\lambda - E_k) + i\delta} \right], \tag{2.57}$$

where $\Phi_{k\lambda}(x) = \langle \Psi_k |\, \hat{\psi}(x)\, | \lambda \rangle$. Equation 2.57 describes the Lehmann representation of the one-particle Green's function. [30]

### 2.4.3 Observables

**Total Energy: Galitskii-Migdal formula**

The total energy is in general a two-body operator and should in principle not be calculable from the one-particle Green's function, but the total energy is an exception to the rule as we will see. We can write down a general expression for the total energy:

$$\begin{aligned} E(z_1) = \langle \Psi |\, \hat{U}(t_{0-}, z_1) \Bigg[ \int dx_1 dx_2\ \hat{\psi}^\dagger(x_1)\, \langle x_1 |\, \hat{h}(z_1)\, | x_2 \rangle\, \hat{\psi}(x_2) \\ + \frac{1}{2} \int dx_1 dx_2\ v(x_1, x_2) \hat{\psi}^\dagger(x_1) \hat{\psi}^\dagger(x_2) \hat{\psi}(x_2) \hat{\psi}(x_1) \Bigg] \hat{U}(z_1, t_{0-})\, | \Psi \rangle\ . \end{aligned} \tag{2.58}$$

Equation 2.58 describes the kinetic energy plus potential energy, in that order. The time-argument on the contour is simply there so that in the next step we can identify the one- and two-particle Green's function. The Hamiltonian has, if any, a real-time dependence.

By definition of the delta function we have

$$f(z_1) = \int dz_2 f(z_1, z_2)\delta(z_1 - z_2),$$

and inserting the unit operators $\hat{U}(z_1, t_{0-})\hat{U}(t_{0-}, z_2)$ and $\hat{U}(z_2, t_{0-})U(t_{0-}, z_2)$ in the first term in equation 2.58, we have:

$$\begin{aligned} \langle\Psi| \Big[ \int dx_1 d2\ \delta(z_1 - z_2)\hat{U}(t_{0-}, z_1)\hat{\psi}^\dagger(x_1)\hat{U}(z_1, t_{0-})\times \\ \times\hat{U}(t_{0-}, z_2)h(1)\hat{U}(z_2, t_{0-})\hat{U}(t_{0-}, z_2)\hat{\psi}(x_2)\hat{U}(z_2, t_{0-})\Big] |\Psi\rangle = \\ = \int dx_1 d2\ h(1,2)\, \langle\Psi|\, \hat{\psi}^\dagger(x_1 z_1)\hat{\psi}(x_2 z_2)\, |\Psi\rangle = \\ = -i \int dx_1 d2\ h(1,2) G(2, 1^+), \end{aligned} \tag{2.59}$$

where we find precisely the definition of the lesser Green's function $G(2, 1^+)$, similarly the second term can be written in terms of $G(1, 2; 1^+, 2^+)$:

$$E(z_1) = -i \int dx_1 d2\ h(1,2)G(2,1^+) - \frac{1}{2}\int dx_1 d2\ v(1,2)G(1,2;1^{++},2^+). \tag{2.60}$$

The particular form of the arguments in the two-particle Green's function in equation 2.60 also shows up in the equation of motion for the one-particle Green's function, and it is this fact that will allow us to find an expression for the total energy in terms of $G(1,2)$ only. If we combine the equation of motion for $G(1,2)$ and its adjoint, and set $2 = 1^+$:

$$\begin{aligned} \left(i\frac{d}{dz_1} - i\frac{d}{dz_2}\right) G(1,2)\Big|_{2=1^+} - \int d3\ \big[h(1,3)G(3,1^+) + G(1,3^+)h(3,1)\big] - \\ = -2i \int d3\ v(1,3)G(1,3;1^{++},3^+). \end{aligned} \tag{2.61}$$

From equation 2.61 we have then found a way to write $G(1,2;1^{++},2^+)$ in terms of $G(1,2)$, where $z_1^{++}$ now is infinitesimally later than $z_1^+$. If we then

insert this into equation 2.60 we find the Galitskii-Migdal [31] formula for the total energy in terms of only the one-particle Green's function:

$$E(t) = -\frac{i}{4}\int dxdx' \left(i\frac{d}{dt}\delta(x,x') - i\frac{d}{dt'}\delta(x,x') + 2h(x,x';t)\right) G(x't,xt')\Big|_{t'=t} \tag{2.62}$$

When the Hamiltonian is time-independent (in a steady state), i.e. $\hat{h}(t) \equiv \hat{h}$, the scenario discussed in this thesis, the Green's function depends only on the difference of times $t - t'$, and we can write the equation in the frequency domain:

$$E = -\frac{i}{2}\int \frac{d\omega}{2\pi}\int dxdx' \left(\omega\delta(x,x') + h(x,x')\right)G(x',x;\omega). \tag{2.63}$$

**Meir-Wingreen formula: Current**

In order to study out of equilibrium dynamics of an open system (see figure 1.1), one can apply a voltage difference over the system. Then, e.g., the left lead has a bias $V_L(t)$ and the right lead is unbiased. The Hamiltonian corresponding to this perturbation is then:

$$\hat{H}(t) = \hat{H}_0 + \hat{H}_{int} + \hat{H}_V(t),\ \hat{H}_V(t) = \sum_{k\in L\sigma} qV_L(t)\hat{n}_{k\sigma}. \tag{2.64}$$

We can then compute the current as the change in the number of particles in the left lead:

$$\hat{I}_{L\sigma}(t) = q\frac{d}{dt}\hat{N}_{L\sigma}(t),\ \hat{N}_{L\sigma}(t) = \sum_{k\in L}\hat{n}_{k\sigma}(t). \tag{2.65}$$

The number operators here are in the Heisenberg picture, so we can compute the derivative using the Heisenberg equation of motion:

$$\frac{d}{dt}\hat{N}_L(t) = i\left[\hat{H}(t), \hat{N}_L(t)\right]. \tag{2.66}$$

For tight-binding leads and contact region and with an interaction of the type $\nu_{ij}^{\sigma\sigma'}\hat{n}_{i\sigma}\hat{n}_{j\sigma'}$, the number operator $\hat{N}_L$ commutes with everything in $\hat{H}(t)$ except the term connecting the left lead to the central region:

$$
\begin{aligned}
i\left[\hat{H}(t),\hat{N}_L\right] &= i\sum_{k\in L}\left[V_{LC}\hat{c}_L^\dagger\hat{c}_1 + V_{LC}^*\hat{c}_1^\dagger\hat{c}_L,\ \hat{n}_k\right] = \\
&= i\sum_k\left[-V_{LC}\hat{c}_L^\dagger\hat{c}_1 + V_{LC}^*\hat{c}_1^\dagger\hat{c}_L\right],
\end{aligned}
\tag{2.67}
$$

where $V_{LC}$ is the hopping matrix element between the left lead and the device system.

If we then take the ensemble average of $\hat{I}_{L\sigma}(t)$:

$$
\langle\hat{I}_{L\sigma}(t)\rangle = -iqV_{LC}\langle\hat{c}_L^\dagger(t)\hat{c}_1(t)\rangle + iqV_{LC}^*\langle\hat{c}_1^\dagger(t)\hat{c}_L(t)\rangle = 2q\Re\{V_{LC}G_{L1}^<(t,t)\}. \tag{2.68}
$$

It is possible to express the quantity $G_{L1}^<$ entirely in terms quantities from the central region, $MM$, and after some algebra [29] we find the Meir-Wingreen formula [32] for the current:

$$
I_{L\sigma}(t) = 2q\Re\{(\Sigma_{L,emb}^<\cdot G_{CC}^A + \Sigma_{L,emb}^R\cdot G_{CC}^< + \Sigma_{L,emb}^\rceil\star G_{CC}^\lceil)(t,t)\}, \tag{2.69}
$$

where $\Sigma_{L,emb}$ is the so-called embedding self-energy which will be described in detail in section 3.1.1.

In a steady state, we can Fourier transform equation 2.69 for a description in the frequency domain:

$$
I_{L\sigma} = 2iq\int\frac{dw}{2\pi}(\Sigma_{L,emb}^<(\omega)A_{CC}(\omega) - \Gamma_{L,emb}(\omega)G_{CC}^<(\omega)). \tag{2.70}
$$

# Chapter 3

# Theoretical Background B

## 3.1 Self-Energies

As we saw previously, the equation of motion for the one-particle Green's function constitutes a hierarchy of equations. The typical way to close the equation is by introducing the so-called self energy:

$$\int d3\ \Sigma(1,3)G(3,2) = -i \int d3\ v(1,3)G(1,3;2,3^{+}). \tag{3.1}$$

The self energy is a functional of the Green's function containing the non-local properties of the two-particle Green's function. We will encounter two different types of self energy below, an embedding self energy and a many body self energy.

### 3.1.1 Embedding Self Energy

Consider a system consisting of a molecule connected to non-interacting one-dimensional reservoirs, or leads, on either side in a manner similar to a chain. If we consider the equation of motion:

$$\left[ i\frac{d}{dz}\mathbf{1} - \mathbf{h}(z) \right] \mathbf{G}(z,z') = \delta(z,z')\mathbf{1} + \int_{\gamma} \mathbf{\Sigma}(z,\bar{z})\mathbf{G}(\bar{z},z'). \tag{3.2}$$

The boldface quantities are now block matrices where each of the blocks are the projection onto the subspace corresponding to the reservoirs, $\alpha =$

$L, R$, or to the molecule. For example:

$$\mathbf{h} = \begin{pmatrix} h_{LL} & h_{LC} & 0 \\ h_{CL} & h_{CC} & h_{CR} \\ 0 & h_{RC} & h_{RR} \end{pmatrix}, \tag{3.3}$$

where the components are again matrices in the respective site basis of the region.

It is important to note that since the leads are non-interacting, the only non-vanishing block of $\mathbf{\Sigma}(z, z')$ is that of the central molecule, $\Sigma_{CC}(z, z')$. Furthermore, the equation of motion for the Green's function of an isolated lead has the simple form:

$$\left[ i\frac{d}{dz} - h_{\alpha\alpha}(z) \right] g_{\alpha\alpha}(z, z') = \delta(z, z'). \tag{3.4}$$

If we write out the remaining projections of the equation 3.2, namely the $CC$ and $\alpha C$ components:

$$\left[ i\frac{d}{dz} - h_{CC}(z) \right] G_{CC}(z, z') = \delta(z, z') + \int_\gamma \Sigma_{CC}(z, \bar{z}) G_{CC}(\bar{z}, z') + \\ + \sum_\alpha h_{C\alpha}(z) G_{\alpha C}(z, z'), \tag{3.5}$$

$$\left[ i\frac{d}{dz} - h_{\alpha\alpha}(z) \right] G_{\alpha C}(z, z') = h_{\alpha C}(z) G_{CC}(z, z'). \tag{3.6}$$

Equation 3.6 can be solved for $G_{\alpha C}(z, z')$ by relabeling $z \to \bar{z}$, multiplying from the left by $g_{\alpha\alpha}(z, \bar{z})$ and integrating over $\bar{z}$.

$$G_{\alpha C}(z, z') = \int d\bar{z} g_{\alpha\alpha}(z, \bar{z}) h_{\alpha C}(\bar{z}) G_{CC}(\bar{z}, z'). \tag{3.7}$$

Plugging this result back into 3.5:

$$\left[ i\frac{d}{dz} - h_{CC}(z) \right] G(z, z') = \delta(z, z') + \int_\gamma \Sigma_{CC}(z, \bar{z}) G_{CC}(\bar{z}, z') + \\ + \sum_\alpha \int_\gamma h_{C\alpha}(z) g_{\alpha\alpha}(z, \bar{z}) h_{\alpha C}(\bar{z}) G_{CC}(\bar{z}, z'), \tag{3.8}$$

where we can now define [26]:

$$\Sigma_{emb}(z, z') = \sum_{\alpha} h_{C\alpha}(z) g_{\alpha\alpha}(z, z') h_{\alpha C}(z'). \tag{3.9}$$

Then we can work with the Green's function solely in the projection on the molecule:

$$[i\partial_z - h(1)]\, \boldsymbol{G}_{CC}(z, z') = \delta(z, z') + \int_{\gamma} d\bar{z}\ (\boldsymbol{\Sigma}_{CC}(z, \bar{z}) + \boldsymbol{\Sigma}_{\text{emb}}(z, \bar{z}))\boldsymbol{G}_{CC}(\bar{z}, z'). \tag{3.10}$$

## 3.2 Many Body Self Energy

The self-energy approach to treating interactions is a perturbative method. The method is based on Feynman diagrams, of which there are infinitely many, and consciously choosing to neglect all but a few typically corresponding to a class of interactions of interest. Feynman diagrams [33] are pictorial representations of, typically, interactions between particles. The diagrams are drawn and interpreted according to the *Feynman rules*.

In this thesis, we treat two types of interactions; Hartree-Fock (HF), a mean-field interaction linear in the interaction strength, and Second Born (2B), the self-energy up to second order in the **bare** interaction. Indeed, there are many more classes of interactions such as e.g. GW [34] and T-matrix [35], but they are not considered here.

### 3.2.1 Hartree-Fock

The HF approximation for the self-energy is the simplest type of interaction, namely mean field. In this approximation, the two-particle Green's function describing the interactions between particles decouples into a product of two one-particle Green's functions:

$$G(1, 3; 2, 3^+) = G(1, 2)G(3, 3^+) - G(1, 3^+)G(3, 2). \tag{3.11}$$

This then becomes a description of non-interacting quasi-particles moving in a potential generated by the rest of the particles. If we insert this into the equation of motion for the Green's function:

$$\left[i\frac{d}{dt_1} - h(1)\right] G(1,2) = \delta(1,2) \\ - i\int d3\ \nu(1,3)(G(1,2)G(3,3^+) - G(1,3^+)G(3,2)), \quad (3.12)$$

we can identify the self-energy:

$$\Sigma_{HF}(1,2) = -i\delta(1-2)\int d3\ \nu(1,3)G(3,3^+) + i\nu(1,2)G(1,2^+). \quad (3.13)$$

Remembering that the interaction is time-local: $\nu(1,2) = \delta(z_1 - z_2)\nu(x_1,x_2)$ we can write the Hartree-Fock self energy as:

$$\Sigma_{HF}(x_1z_1,x_2z_2) = \delta(x_1,x_2)\delta(z_1,z_2)\int dx_3\nu(x_1,x_3)G(x_3z_1,x_3z_1^+) \\ - \nu(x_1,x_2)G(x_1z_1,x_2z_1^+). \quad (3.14)$$

We can use the Langreth rules find the retarded and lesser components of $\Sigma_{HF}$:

$$\Sigma^R_{HF}(x_1t_1,x_2t_2) = \delta(x_1,x_2)\delta(t_1-t_2)\int dx_3\ \nu(x_1,x_3)G^<(x_3t_1,x_3t_1^+) \\ -\nu(x_1,x_2)G^<(x_1t_1,x_2t_1^+), \quad (3.15)$$

$$\Sigma^<_{HF} \equiv 0. \quad (3.16)$$

Equation 3.15 makes it clear that in the Hartree-Fock approximation particles interact with the potential generated by all the other particles. From a diagrammatic point of view, the Hartree-Fock approximation is the partial sum of the two non-reducible diagrams of first order in the interaction, see figure 3.1.

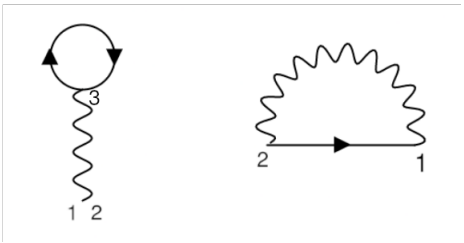


Figure 3.1: The Feynamn diagrams corresponding to the HF approximation.

### 3.2.2 Second Born

Unlike the Hartree-Fock approximation, the 2B approximation includes particle-particle scatterings to first order. The simplest direct scattering that can occur is the process where two particles are injected at $1'$ and $2'$, interact (scatter) at $\bar{1}$ and $\bar{2}$ respectively, and are removed at 1 and 2. This corresponds to approximating the two-particle Green's function as:

$$G_{\text{direct}}(1,2;2',1') = \int d\bar{1}d\bar{2}\ \nu(\bar{1},\bar{2})G(1,\bar{1})(\bar{1},1')G(2,\bar{2})G(\bar{2},2'). \tag{3.17}$$

We must also include the exchange term, to comply with the anti-symmetry of $G^{(2)}$, which corresponds to $1' \leftrightarrow 2'$:

$$G(1,2;2',1') = G_{HF}(1,2,2',1) + \int d\bar{1}d\bar{2}\ \nu(\bar{1},\bar{2})\left[G(1,\bar{1})(\bar{1},1')G(2,\bar{2})G(\bar{2},2')\right.$$
$$\left. -G(1,\bar{1})G(\bar{1},2')G(2,\bar{2})G(\bar{2},1')\right]. \tag{3.18}$$

Again, plugging this into the equation of motion:

$$\left[i\frac{d}{dt_1} - h(1)\right]G(1,2) = \delta(1,2) + \int d3\ \left\{\Sigma^{HF}(1,3^+)G(3,2)\right.$$
$$-i\nu(1,3)\int d4d5\ \nu(4,5)\left[G(1,4)G(4,2)G(3,5)G(5,3^+)\right.$$
$$\left.\left. -G(1,4)G(4,3^+)G(3,5)G(5,2)\right]\right\}. \tag{3.19}$$

From equation 3.19 it is not at all obvious, unlike in HF, what form the self-energy has. For more complicated interactions than HF, this process becomes very tedious and unsystematic. Instead, we turn to Feynman diagrams. They allow us to systematically find the self-energy for in principle arbitrary interaction. We find their root in the expansion of the one-particle Green's function in powers of the interaction $\nu(1,2)$ [26]:

$$G(a,b) = \frac{\sum_{k=0}^{\infty} \frac{1}{k!} \left(\frac{i}{2}\right)^2 \int d1d1'..dkdk' v(1,1')..v(k,k') \begin{vmatrix} G_0(a,b) & G_0(a,1^+) & ... & G_0(a,k'^+) \\ G_0(1,b) & G_0(1,1^+) & ... & G_0(1,k'^+) \\ \vdots & \vdots & \ddots & \vdots \\ G_0(k,b) & G_0(k,1^+) & ... & G_0(k,k'^+) \end{vmatrix}}{\sum_{k=0}^{\infty} \frac{1}{k!} \left(\frac{i}{2}\right)^2 \int d1d1'..dkdk' v(1,1')..v(k,k') \begin{vmatrix} G_0(1,1^+) & G_0(1,1^+) & ... & G_0(1,k'^+) \\ G_0(1',1^+) & G_0(1',1'^+) & ... & G_0(1',k'^+) \\ \vdots & \vdots & \ddots & \vdots \\ G_0(k,1^+) & G_0(k,1'^+) & ... & G_0(k,k'^+) \end{vmatrix}}. \tag{3.20}$$

The Feynman rules then dictate how to convert between graphical diagrams and terms appearing in equation 3.20. For a detailed discussion on Feynman diagrams and their rules, see e.g. [33]. We will mention the relevant rules for our purposes here:

1. An oriented line represents the bare propagator $G_0(1,2)$

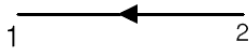


2. A wiggly line represents an interaction $v(1,2)$

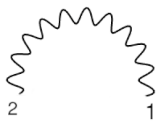


3. Disconnected diagrams, i.e. diagrams with open-ended propagators, do not contribute

4. Topologically equivalent diagrams have the same self-energy

5. Internal vertices are integrated over

To that end, the diagrams that are needed to construct the many-body self-energy are the irreducible diagrams, i.e. connected inequivalent diagrams. The second born approximation for the self-energy includes all diagrams up to second order in the interaction, which are the four in figure 3.2.

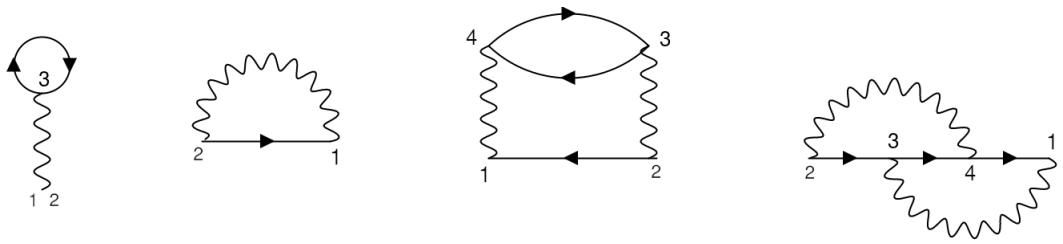


Figure 3.2: The Feynman diagrams corresponding to the 2B approximation.

To convert the diagrams in figure 3.2 to an analytical expression, we convert oriented lines to propagators, wiggly lines to interactions and integrate over the internal vertices:

$$\Sigma_{2B}(1,2) = \Sigma_{HF}(1,2) + \int d3d4 \;\; [G(1,2)\nu(2,3)G(3,4)G(4,3)\nu(4,1) \\ -G(1,4)G(4,3)\nu(4,2)G(3,2)\nu(3,1)] \,. \tag{3.21}$$

Again, the interactions are time-local:

$$\Sigma_{2B}(x_1 z_1, x_2 z_2) = \Sigma_{HF}(x_1 z_2, x_2 z_2) \\ + \int dx_3 dx_4 \, [G(x_1 z_1, x_2 z_2)\nu(x_2, x_3)G(x_4 z_2, x_3 z_1)G(x_3 z_1, x_4 z_2)\nu(x_4, x_1) \\ -G(x_1 z_1, x_4 z_2)G(x_4 z_2, x_3 t_1)\nu(x_4, x_2)G(x_3 t_1, x_2 z_2)\nu(x_3, x_1)] \,. \tag{3.22}$$

We can then use the Langreth rules to find the retarded and lesser components of $\Sigma_{2B}$:

$$
\begin{aligned}
\Sigma^R_{2B}(x_1t_1, x_2t_2) &= \Sigma^R_{HF}(x_1t_1, x_2t_2) \\
&+ \int dx_3dx_4 \, \{ \\
\nu(x_4, x_1)\nu(x_2, x_3) \, &\big[G^R(x_1t_1, x_2t_2)G^<(x_4t_2, x_3t_1)G^>(x_3t_1, x_4t_2) \\
&+G^<(x_1t_1, x_2t_2)G^A(x_4t_2, x_3t_1)G^<(x_3t_1, x_4t_2) \\
&+G^<(x_1t_1, x_2t_2)G^<(x_4t_2, x_3t_1)G^R(x_3t_1, x_4t_2)\big] \\
-\nu(x_4, x_2)\nu(x_3, x_1) \, &\big[G^R(x_1t_1, x_4t_2)G^<(x_4t_2, x_3t_1)G^>(x_3t_1, x_2t_2) \\
&+G^<(x_1t_1, x_4t_2)G^A(x_4t_2, x_3t_1)G^<(x_3t_1, x_2t_2) \\
&+G^<(x_1t_1, x_4t_2)G^<(x_4t_2, x_3t_1)G^R(x_3t_1, x_2t_2)\big] \big\} \, .
\end{aligned}
\tag{3.23}
$$

In a steady state, all quantities in equation 3.23 depend on the time-difference $t = t_1 - t_2$. We can then Fourier transform the $\Sigma^R_{2B}$:

$$
\begin{aligned}
\Sigma^R_{2B}(x_1, x_2; \omega) &= \Sigma^R_{HF}(x_1, x_2; \omega) \\
&+ \int dx_3dx_4 \int \frac{d\omega' d\omega''}{(2\pi)^2} \, \{ \\
\nu(x_4, x_1)\nu(x_2, x_3) \, &\big[G^R(x_1, x_2; \omega')G^<(x_4, x_3; \omega'')G^>(x_3, x_4; \omega - \omega' + \omega'') \\
&+G^<(x_1, x_2; \omega')G^A(x_4, x_3; \omega'')G^<(x_3, x_4; \omega - \omega' + \omega'') \\
&+G^<(x_1, x_2; \omega')G^<(x_4, x_3; \omega'')G^R(x_3, x_4; \omega - \omega' + \omega'')\big] \\
-\nu(x_4, x_2)\nu(x_3, x_1) \, &\big[G^R(x_1, x_4; \omega')G^<(x_4, x_3; \omega'')G^>(x_3, x_2; \omega - \omega' + \omega'') \\
&+G^<(x_1, x_4; \omega')G^A(x_4, x_3; \omega'')G^<(x_3, x_2; \omega - \omega' + \omega'') \\
&+G^<(x_1, x_4; \omega')G^<(x_4, x_3; \omega'')G^R(x_3, x_2; \omega - \omega' + \omega'')\big] \big\} \, .
\end{aligned}
\tag{3.24}
$$

By a similar process we can find the lesser component:

$$
\begin{aligned}
\Sigma^<_{2B}(x_1, x_2; \omega) &= \int dx_3dx_4 \int \frac{d\omega' d\omega''}{(2\pi)^2} \, [ \\
&\nu(x_1, x_4)\nu(x_2, x_3)G^<(x_1, x_2; \omega')G^>(x_4, x_3; \omega'')G^<(x_3, x_4; \omega - \omega' + \omega'') \\
-\nu(x_2, x_4)\nu(x_1, x_3) &G^<(x_1, x_4; \omega')G^>(x_4, x_3; \omega'')G^<(x_3, x_2; \omega - \omega' + \omega'')] \, .
\end{aligned}
\tag{3.25}
$$

### 3.2.3 Non-perturbative Self-Energy

We can make some observations about the self-energy, notably that the exact self-energy can be readily obtained from the exact one- and two-particle

Green's function:

$$\boldsymbol{\Sigma}(\omega) = \boldsymbol{G}_0^{-1}(\omega) - \boldsymbol{G}^{-1}(\omega), \tag{3.26}$$

$$\Sigma(1,4) = -i \int d2d3 \; v(1,3) G(1,3;2,3^+) G^{-1}(2,4), \tag{3.27}$$

$$\Sigma(x_1, x_4; \omega) = -i \int dx_2 dx_3 G(x_1, x_3; x_2, x_3; \omega) G^{-1}(x_2, x_4; \omega), \tag{3.28}$$

where $\boldsymbol{G}_0$ is the non-interacting Green's function, and equation 3.28 is the Fourier transform of equation 3.27 keeping in mind that $v(1,3)$ is time-local, reducing the time-dependence of the two-particle Green's function to only $t_1, t_2$. Note that equation 3.26 is not necessarily true out of equilibrium, however we will apply it to equilibrium systems.

# Chapter 4

# Method

## 4.1 Numerical implementation

A large portion of the outcome of this thesis was dedicated to implementing a codebase for performing simulations using the NEGF method in a steady state. The codebase for performing calculations in open systems was written in FORTRAN, whereas the calculation of the non-perturbative self-energy was written in Julia.

Below we outline crucial aspects of the codebase.

- **Numerically calculate non-equilibrium Green's function in open (infinite) systems.**

  In a non-interacting scenario, this amounts to calculating the embedding self-energy and solve the Dyson equation, by inversion, in the frequency space. For interacting particles, the calculation needs to be self-consistent:

  1. Calculate embedding self-energy and non-interacting $\mathbf{G}(\omega)$
  ↓
  2. Calculate one-particle density matrix and perform the Fourier integrals for $\Sigma_{2B}$
  ↓
  3. Recalculate the Green's function with the new $\Sigma_{MB}$
  ↓
  4. Compare new Green's function to previous, if not close repeat from 2.

- **Fourier transforms for $\Sigma_{2B}$**

  As we saw in section 3.2.2, the second born approximation for the self-energy, in frequency space, involves computing convolutions and cross-correlation, at each iteration. We employ the FFTW [36] framework which provides straightforward routines to compute Fast Fourier Transforms. A typical size of the $\omega$-grid is $2^{15}$, and the number of Fourier integrals required to compute $\Sigma_{2B}$ is $16N_{cc}^2$ where $N_{cc}$ is the size of the interacting region.

- **Optimizing functions**

  The method in section 3.2.3 was implemented in Julia and the minimizer we used utilized the Nelder-Maed algorithm [37], which is based on a simplex algorithm.

All in all, the codebase consists of roughly 2500 lines of code, and what effectively amounts to a library for computing NEGF's in steady state.

The code has been tested, and verified, by comparing results to existing results in the literature [38, 39] and existing code.

# Chapter 5

# The models

## 5.1 Tight-binding chain

The system that will primarily be studied here is one of a chain consisting of an interacting two-site molecule coupled to non-interacting tight-binding leads on either side, see figure 5.1.

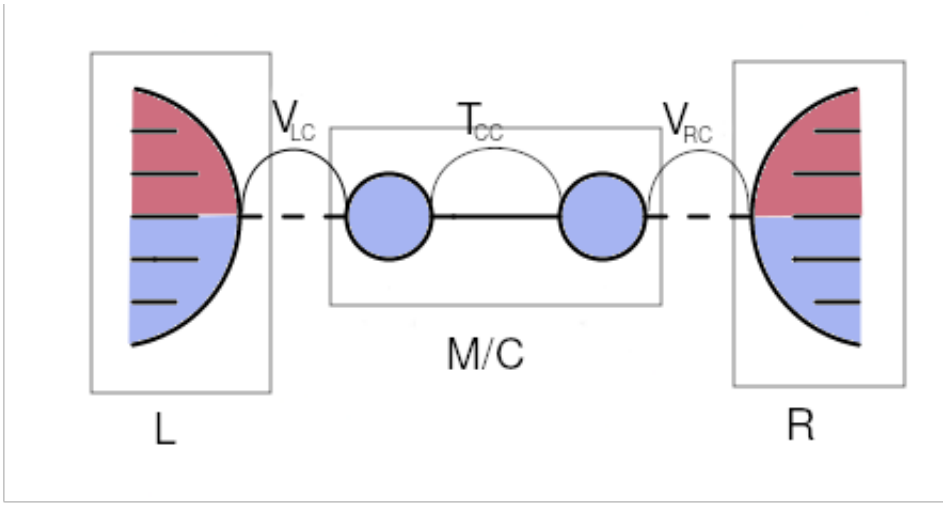


Figure 5.1: Depiction of generic transport system.
"L": Left lead, "M/C": Molecule/Center, "R": Right lead
"$V_{LC}$": Hopping from L to M/C, "$V_{RC}$": Hopping from R to M/C,
"$T_{CC}$": Hopping between sites in Molecule/Center.

The Hamiltonian describing the system is:

$$\hat{H}(t) = \sum_{i\sigma} \epsilon_{i\sigma}\hat{n}_{i\sigma} + \sum_{k\alpha\sigma}(\epsilon_{k\alpha\sigma} + U_\alpha(t))\hat{n}_{k\alpha\sigma} + T_{CC}\sum_{<ij>\sigma}(\hat{c}^\dagger_{i\sigma}\hat{c}_{j\sigma} + \text{H.c.})$$
$$+ T_{\alpha\alpha}\sum_{<mn>\alpha\sigma}(\hat{c}^\dagger_{m\alpha\sigma}\hat{c}_{n\alpha\sigma} + \text{H.c.}) + \sum_{ik\alpha\sigma}(V_{i\sigma,k\alpha\sigma}\hat{c}^\dagger_{i\sigma}\hat{c}_{k\alpha\sigma} + V_{k\alpha\sigma,i\sigma}\hat{c}^\dagger_{k\alpha\sigma}\hat{c}_{i\sigma})$$
$$+ \frac{1}{2}\sum_{ijkl;\sigma\sigma'} w^{\sigma\sigma'}_{ijkl}\ \hat{c}^\dagger_{i\sigma}\hat{c}^\dagger_{k\sigma'}\hat{c}_{j\sigma'}\hat{c}_{l\sigma}, \tag{5.1}$$

where the indices $ijkl$ belong the central molecule, $\alpha$ indicates either left or right lead and $m, n$ belonging to the corresponding lead,

## 5.2 Interacting Ring

This system serves the purpose of a testing grounds for two different scenarios. We use it to study the effect of currents on the Galitskii-Migdal formula and its relationship to correlation functions as well as to test whether the two-particle Green's function computed in a subsystem can be used to construct the self-energy.

### 5.2.1 Flux threaded ring

The method of calculating the correlation function from the Galitskii-Migdal formula involves computing the total energy of a system possibly affected by an electron current, and its numerical derivative. When studying a system connected to infinite leads, any small change of parameters in the contacted system (as needed by the numerical derivative) could potentially be spread far into the leads by the current. By studying a finite system instead, we can make observations as to how a parameter perturbation at an impurity might be affect by currents. One such finite system that can still contain currents is a tight-binding ring threaded by a magnetic flux. Such a system will sustain persistent currents through the ring. [40, 41] We can write the Hamiltonian of a length $L$ tight-binding ring with a magnetic flux through it and an impurity at site $L/2$. We expect to find discrepancies even at the HF level of interaction and hence for computational sake we will use the HF approximation here:

$$\hat{H} = \sum_{i\sigma} \epsilon_{i\sigma} \hat{n}_{i\sigma} + t \sum_{<ij>\sigma} (e^{i\theta} c^{\dagger}_{i\sigma} c_{j\sigma} + \text{H.c.}) + U \hat{n}_{L/2\sigma} \langle \hat{n}_{L/2\bar{\sigma}} \rangle \,. \tag{5.2}$$

The complex phase on the hopping term contains the effect of the magnetic flux. For a detailed discussion of how the Hamiltonian in equation 5.2 is obtained, see [41]. The important thing here is that we can work with a finite system with currents.

To calculate the current flowing through site $k$:

$$\hat{j}_k(t) = q \frac{d}{dt} \hat{n}_k(t) = iq \left[ \hat{H}, \hat{n}_k(t) \right] = 2iqt \sum_{<ij>} (e^{i\theta} \hat{c}^{\dagger}_i \delta_{kj} \hat{c}_j + e^{-i\theta} \hat{c}^{\dagger}_k \delta_{kj} \hat{c}_i), \tag{5.3}$$

where the factor 2 comes from summing over spin, $q$ is the charge of the occupying particles and $t$ the hopping. The current is then the ground state, $|g\rangle$, average of the operator in equation 5.3:

$$\begin{aligned} j_k(t) = 2qt \sum_{<ij>} \sum_{\lambda \in N_{occ}} \delta_{kj} (ie^{i\theta} \langle g | \hat{c}^{\dagger}_i(t) | \lambda \rangle \langle \lambda | \hat{c}_k(t) | g \rangle \\ + ie^{-i\theta} \langle g | \hat{c}^{\dagger}_k(t) | \lambda \rangle \langle \lambda | \hat{c}_i(t) | g \rangle) = 2qt \sum_{\lambda \in N_{occ}} \Im \langle g | (\hat{c}^{\dagger}_{k+1} + \hat{c}^{\dagger}_{k-1} | \lambda \rangle \langle \lambda | \hat{c}_k | g \rangle \,. \end{aligned} \tag{5.4}$$

# Chapter 6

# Results

We divide the presentation of the original results of this thesis into two parts: formal developments and numerical results.

## 6.1 Formal Results

### 6.1.1 Exact Self-Energy

From the definition of the self-energy we saw that with an exact one- and two-particle Green's function we can compute the self-energy. Of course, with the exact one- and two-particle Green's function we already have the complete knowledge of the system, however consider the case of the infinite tight-binding chain with a contacted region in the center. Here it is clearly not possible to compute the exact one- and two-particle Green's function but perhaps computing the two-particle Green's function in a mimicked subsystem provides a good approximation.

In this section, we study a finite interacting ring in order to determine whether a two-particle Green's function on a subsystem containing an impurity can accurately represent the full system.

The Hamiltonian here is:

$$\hat{H} = \sum_{i\sigma} \epsilon_i \hat{n}_{i\sigma} + t \sum_{<ij>\sigma} (c^\dagger_{i\sigma} c_{j\sigma} + \text{H.c.}) + \sum_{i\sigma} U_i \hat{n}_{i\sigma} \hat{n}_{i\bar{\sigma}}. \tag{6.1}$$

The system is in equilibrium and time-independent, so we can easily compute the one-particle Green's function in the Lehmann representation and site basis:

$$G_{ij}(\omega) = \sum_\lambda \frac{\langle\Psi_0|\,\hat{c}_i\,|\lambda\rangle\,\langle\lambda|\,\hat{c}_j^\dagger\,|\Psi_0\rangle}{\omega - (\epsilon_\lambda - \epsilon_0) + i\eta} + \sum_\lambda \frac{\langle\Psi_0|\,\hat{c}_j^\dagger\,|\lambda\rangle\,\langle\lambda|\,\hat{c}_i\,|\Psi_0\rangle}{\omega + (\epsilon_\lambda - \epsilon_0) - i\eta}. \tag{6.2}$$

The two-particle Green's function that is needed in equation 2.50 is $G(1,3;2,3^+)$, however we can note that the interaction $v(1,3)$ is time-local so in fact the two-particle Green's function only depends on $t$ and $t'$:

$$\begin{aligned} G(x_1t, x_3t; x_2t', x_3t^+) = &-\langle\Psi_0|\,\mathcal{T}[\hat{\psi}(x_1t)\hat{\psi}(x_3t)\hat{\psi}^\dagger(x_3t^+)\hat{\psi}^\dagger(x_2t')]\,|\Psi_0\rangle = \\ &= \theta(t-t')\,\langle\Psi_0|\,\hat{\psi}^\dagger(x_3t^+)\hat{\psi}(x_3t)\hat{\psi}(x_1t)\hat{\psi}^\dagger(x_2t')\,|\Psi_0\rangle \\ &-\theta(t'-t)\,\langle\Psi_0|\,\hat{\psi}^\dagger(x_2t')\hat{\psi}^\dagger(x_3t^+)\hat{\psi}(x_3t)\hat{\psi}(x_1t)\,|\Psi_0\rangle\,. \end{aligned} \tag{6.3}$$

Now, here we can expand the Heisenberg operators in much the same way as for the one-particle Green's function, and to connect to $G$ we will write $G^{(2)}$ in the site basis too:

$$\begin{aligned} G_{ikjk}(t,t') = &\,\theta(t-t')e^{i\epsilon_0(t-t')}\,\langle\Psi_0|\,\hat{c}_i\hat{c}_k\hat{c}_k^\dagger e^{-i\hat{H}(t-t')}\hat{c}_j^\dagger\,|\Psi_0\rangle \\ &-\theta(t'-t)e^{-i\epsilon_0(t-t')}\,\langle\Psi_0|\,\hat{c}_j^\dagger e^{i\hat{H}(t-t')}\hat{c}_k^\dagger\hat{c}_k\hat{c}_i\,|\Psi_0\rangle\,. \end{aligned} \tag{6.4}$$

The structure here is very similar to that of the one-particle Green's function, and we can use the same Fourier transform:

$$G_{ikjk}(\omega) = i\sum_\lambda \frac{\langle\Psi_0|\,\hat{c}_k^\dagger\hat{c}_k\hat{c}_i\,|\lambda\rangle\,\langle\lambda|\,\hat{c}_j^\dagger\,|\Psi_0\rangle}{\omega - (\epsilon_\lambda - \epsilon_0) + i\eta} + i\sum_\lambda \frac{\langle\Psi_0|\,\hat{c}_j^\dagger\,|\lambda\rangle\,\langle\lambda|\,\hat{c}_k^\dagger\hat{c}_k\hat{c}_i\,|\Psi_0\rangle}{\omega + (\epsilon_\lambda - \epsilon_0) - i\eta}. \tag{6.5}$$

The purpose of this section is then to see if it is feasible to compute the two-particle Green's function in some subsystem around an impurity and use it to compute a self-energy and in turn the one-particle Green's function.

To be more explicit, consider a ring of 8 sites with an impurity at site 4, occupied by two particles of opposite spin. The one-particle Hamiltonian in the site basis of the ring is then:

$$h = \begin{pmatrix} 0 & -1 & 0 & 0 & 0 & 0 & 0 & -1 \\ -1 & 0 & -1 & 0 & 0 & 0 & 0 & 0 \\ 0 & -1 & 0 & -1 & 0 & 0 & 0 & 0 \\ 0 & 0 & -1 & U & -1 & 0 & 0 & 0 \\ 0 & 0 & 0 & -1 & 0 & -1 & 0 & 0 \\ 0 & 0 & 0 & 0 & -1 & 0 & -1 & 0 \\ 0 & 0 & 0 & 0 & 0 & -1 & 0 & -1 \\ -1 & 0 & 0 & 0 & 0 & 0 & -1 & 0 \end{pmatrix}. \tag{6.6}$$

We can compute the exact interacting and non-interacting one-particle Green's function from equation 6.2 and hence also the exact self-energy. We know from the diagrammatic expansion of the self-energy that the interaction lines start and end on interacting sites, i.e. only combinations of sites that interact have corresponding non-zero elements of the self-energy in the site basis. In this particular example, the only interacting site is site 4 with a Hubbard interaction, hence the only non-zero element of the self-energy is $\Sigma_{4,4}$.

If we were to compute the two-particle Green's function in a system consisting only of the impurity and use equation 3.28 with the appropriately sized $G$ the resulting self-energy would be an approximation of the true self-energy, however poor. Perhaps a subsystem of three sites with one impurity is a better approximation, or five.

The purpose here is to numerically test the feasibility of this method; to quantify how "poor" of an approximation the subsystem self-energy is we define a norm function:

$$f(\mathcal{S}) = \sum_{ij} \int d\omega |\Sigma_{ij}^{\text{true}}(\mathcal{S};\omega) - \Sigma_{ij}^{\text{approx}}(\mathcal{S};\omega)|^2. \tag{6.7}$$

For a given system, the function $f$ is then to be minimized over some parameter space $\mathcal{S}$.

### 6.1.2 Two-body correlation functions

From the equation of motion of the Green's function, it is possible to construct a density-density correlation function in the special case where the interaction is purely local, i.e. $v(1,2) = v(1,1)\delta(1-2)$.

$$\left[i\frac{d}{dz_1} - h(1)\right] G(1,2) = \delta(1,2) - i\int d3\ v(1,3)G^{(2)}(1,3,2,3^+). \tag{6.8}$$

The typical way of closing these equations is to introduce the self-energy, a quantity which contains all the two-particle interactions otherwise described by the two-particle Green's function:

$$\int d3\ \Sigma(1,3)G(3^+,2) = -i\int d3\ v(1,3)G^{(2)}(1,3,2,3^+). \tag{6.9}$$

Writing out the arguments explicitly and taking into account that the interaction is time-local: $v(x_1t_1, x_2t_2) = v(x_1,x_2)\delta(t_1-t_2)$

$$\begin{aligned}\int dx_3dt_3\ \Sigma(x_1t_1,x_3,t_3)G(x_3t_3^+,x_2t_2) = \\ = -i\int dx_3\ v(x_1,x_3)G^{(2)}(x_1t_1,x_3t_1,x_2t_2,x_3t_1^+).\end{aligned} \tag{6.10}$$

With a quick look at the definition of the two-particle Green's function:

$$G^{(2)}(1,2,3,4) = \frac{1}{i^2}\left\langle \mathcal{T}\hat{\psi}(1)\hat{\psi}(2)\hat{\psi}^\dagger(4)\hat{\psi}^\dagger(3)\right\rangle, \tag{6.11}$$

one can see that if $x_3t_3 = x_1t_1^+$ and $x_4t_4 = x_2t_2^+$ then we have precisely, less a minus sign, the two-particle correlation function: $\langle\hat{n}(1)\hat{n}(2)\rangle$.

To illustrate both the usefulness and downfall of this approach, consider a two-site molecule:

$$H = \sum_{i\sigma}\epsilon_i\hat{n}_{i\sigma} + t\sum_{<ij>\sigma}(\hat{a}^\dagger_{i\sigma}\hat{a}_{j\sigma} + \text{H.c.}) + \sum_{ij\sigma\sigma'}v_{ij}^{\sigma\sigma'}\hat{n}_{i\sigma}\hat{n}_{j\sigma'}. \tag{6.12}$$

With no assumptions on the structure of $v_{ij}^{\sigma\sigma'}$ one would have:

$$\sum_{k\sigma''}\int dt_3\ \Sigma_{ik}^{\sigma\sigma''}(t_1,t_3)G_{kj}^{\sigma''\sigma'}(t_3^+,t_2) = \sum_{k\sigma''} -iv_{ik}^{\sigma\sigma''}G_{ikjk}^{\sigma\sigma''\sigma'\sigma''}(t_1,t_1,t_2,t_1^+). \tag{6.13}$$

It is clear that no useful information can be extracted from equation 6.13 due to the ambiguity of $v_{ik}^{\sigma\sigma''}$. However, when considering a purely local interaction, i.e. allowing only local on-site interactions, $v_{ij}^{\sigma\sigma'} = v_{ij}^{\sigma\sigma'}\delta_{ij}\delta_{\sigma'\bar{\sigma}}$:

$$\sum_{k\sigma''} \int dt_3 \; \Sigma_{ik}^{\sigma\sigma''}(t_1, t_3) G_{kj}^{\sigma''\sigma'}(t_3^+, t_2) = -i v_{ii}^{\sigma\bar{\sigma}} G_{iiji}^{\sigma\bar{\sigma}\sigma'\bar{\sigma}}(t_1, t_1, t_2, t_1^+). \tag{6.14}$$

Now if we set $j = i$, $\sigma' = \sigma$ and $t_2 = t_1^+$, we have on the right-hand side of equation 6.14 the correlation function:

$$\langle n_{i\sigma} n_{i\bar{\sigma}} \rangle = \frac{i}{v_{ii}^{\sigma\bar{\sigma}}} \sum_{k\sigma''} \int dt_3 \; \Sigma_{ik}^{\sigma\sigma''}(t_1, t_3) G_{ki}^{\sigma''\sigma}(t_3^+, t_1^+). \tag{6.15}$$

This can be a powerful tool when considering systems with strong local interaction and weak non-local interaction where the non-local part can be neglected, however for more general types of interactions a different approach is needed.

An alternative *and novel*, approach we have found is to use the Hellman-Feynman theorem in combination with the Galitskii-Migdal formula for the total energy.

The Hellman-Feynman theorem states that:

$$\frac{dE_\lambda}{d\lambda} = \langle \psi_\lambda | \frac{d\hat{H}_\lambda}{d\lambda} | \psi_\lambda \rangle , \tag{6.16}$$

where $\lambda$ is some parameter that appears in the Hamiltonian. In the case of the interacting two-site molecule, the Hamiltonian is:

$$\hat{H}_C = t \sum_{<ij>\sigma} (\hat{a}_{i\sigma}^\dagger \hat{a}_{j\sigma} + \text{H.c.}) + \sum_{ij\sigma\sigma'} v_{ij}^{\sigma\sigma'} \hat{n}_{i\sigma} \hat{n}_{j\sigma'}. \tag{6.17}$$

If we substitute the Hamiltonian in equation 6.16 and let $\lambda$ be anyone of the matrix elements of $v_{ij}^{\sigma\sigma'}$, the derivative will pick up the corresponding term. For example, if we let $\lambda = v_{11}^{+-}$ then:

$$\frac{dE}{dv_{11}^{+-}} = \langle n_{1+} n_{1-} \rangle . \tag{6.18}$$

Then, depending on the correlation function of interest one performs a numerical derivative with respect to the specific interaction matrix element.

An example:
Choose parameters → Self consistency → Compute total energy $E_1 \rightarrow v_{11}^{+-} = v_{11}^{+-} + \delta v$
→ Self consistency → Compute total energy $E_2$, then:

$$\langle \hat{n}_{1+} \hat{n}_{1-} \rangle = \frac{E_2 - E_1}{\delta v}. \tag{6.19}$$

While this new procedure to find correlations is rather simple on paper, its numerical implementation introduces significant complications, since now one must in principle adopt a spinor formulation. Furthermore, additional care is needed when studying a system consisting of a "molecule" connected to semi-infinite leads. In this case the subtraction of the two energies pertains to two infinite systems (each of them with a lead-device-lead structure.)

## 6.2 Numerical Results

### 6.2.1 Non-Interacting Concurrence

This section serves as a means of verifying our code with analytical results [19]. Furthermore, with a numerical solution we can test the approximations made in order to obtain the analytical results. We, like the study in [19], examine the generic quantum transport system in 1.1, with a hamiltonian as in equation 5.1. The parameters used here are: $\epsilon = 1$, $T_{CC} = 0.002$, $\omega_{ijkl} \equiv 0$. We employ the wide-band limit: $\Sigma^R_{\alpha,emb} \rightarrow -i\frac{\Gamma}{2}$, with $\Gamma = 0.01$.

Figure 6.1: The numerical equivalent of the calculation done in figure a) of [19], with and without the approximation $f(\omega) \equiv f(\epsilon)$ respectively.

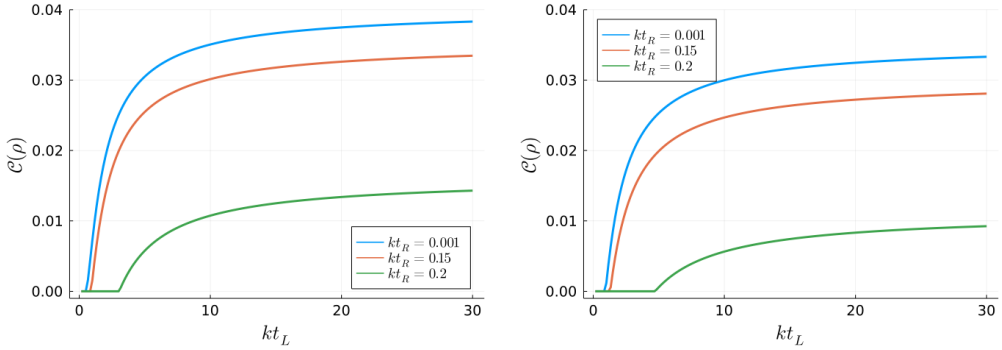


1) Constant $f_{L/R}(\omega)$ 2) Exact $f_{L/R}(\omega)$

Figure 1) in 6.1 represents the result obtained by our numerical implementation of NEGF and perfectly reproduces the analytical results in figure a) from [19]. Figure 2) in 6.1 shows the result from a near identical calculation except where the exact Fermi-Dirac distribution is used. The concurrences in the different scenarios are similar, with 2) displaying a slight overall decrease in concurrence between the quantum dots, indicating that the approximation $f(\omega) \equiv f(\epsilon)$ is appropriate.

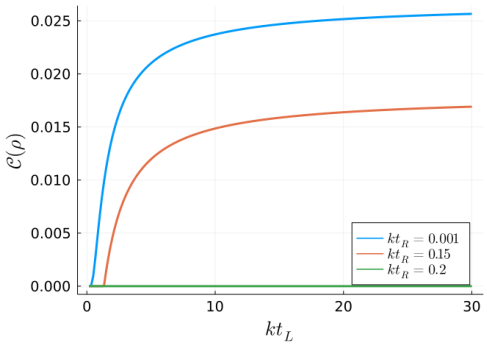


Figure 6.2: Numerical equivalent of figure b) in [19].

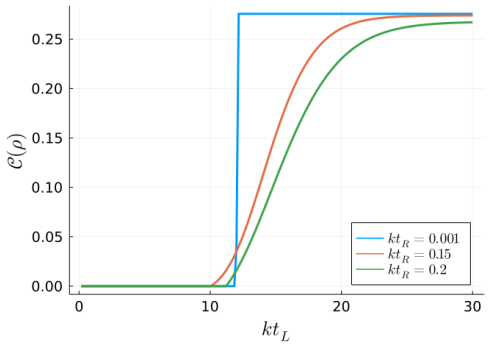


Figure 6.3: Numerical equivalent of figure c) in [19].

Figures 6.1, 6.2 and 6.3 show that our implementation of the NEGF method works as intended.

### 6.2.2 Galitskii-Migdal; effect of current

We saw in section 6.1.2 that we can compute two-body correlation functions by use of the Galitskii-Migdal formula. Here we investigate what effect a current has on this method.

We will work with the setup in section 5.2.1 which allows us to study a finite system with currents present. We choose vanishing on-site energies, i.e. $\epsilon_i = 0 \ \forall i$ and the nearest-neighbor hopping integral is taken to be -1. The concerns lifted in section 6.1.2, with open systems are not present here.

We work in equilibrium, so that all the ensemble averages are over the ground state. This allows us to easily verify what the exact correlation function is: by diagonalizing $\hat{H}$ in the basis $\{|\psi_m\rangle = \hat{c}^\dagger_{i+}\hat{c}^\dagger_{j-}|0\rangle\}$. If we, for example, are computing the $\langle \hat{n}_{4+}\hat{n}_{4-}\rangle$ then the exact correlation function

is the coefficient of the basis state $|\psi_p\rangle = \hat{c}^\dagger_{4+}\hat{c}^\dagger_{4-}|0\rangle$ in the ground state, squared.

We start from a non-interacting ring of length $L = 10$, with the Hamiltonian from section 5.2.1 occupied by two electrons with opposite spin. In the non-interacting case, the system is uniform and as such the density at each site is just $n_{i\sigma} = N_\sigma/L$, where $N_\sigma$ is the number of particles in the system with spin $\sigma$. The correlation function $\langle \hat{n}_{i+}\hat{n}_{j-}\rangle$ factorizes, when non-interacting, into $\langle \hat{n}_{i+}\rangle \langle \hat{n}_{j-}\rangle \equiv N_\sigma^2/L^2 = 1^2/10^2 = 0.01$.

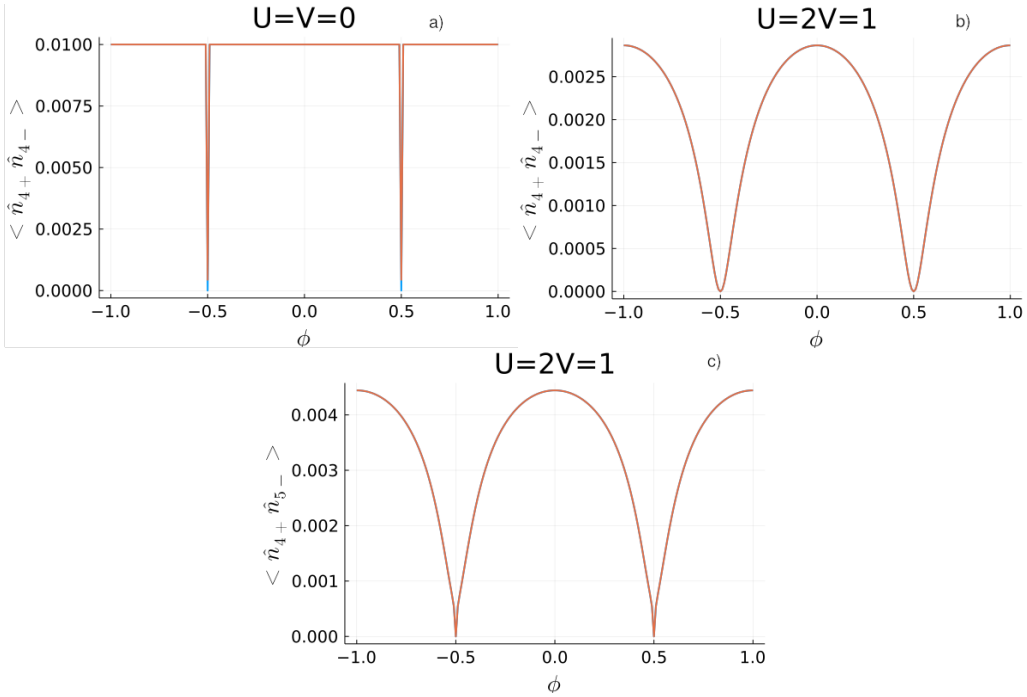


Figure 6.4: The dependence of the interacting and non-interacting correlation functions with $\phi = \theta/2\pi$ in a 10-site ring with an impurity at site 4. The exact ground state average (blue) behind the results from GM method (orange)

In figure 6.4 we display the different correlation functions computed exactly and via the GM formula. For values of $\phi \in (-1, 1)\backslash 0$, the system exhibits currents. To compute the derivative, we used the forward difference with a step size of $h = 10^{-6}$. The discontinuities at $\phi = \pm\frac{1}{2}$ in figure a) in 6.4 are the result of a cusp in the total energy at that point, see figure 6.5

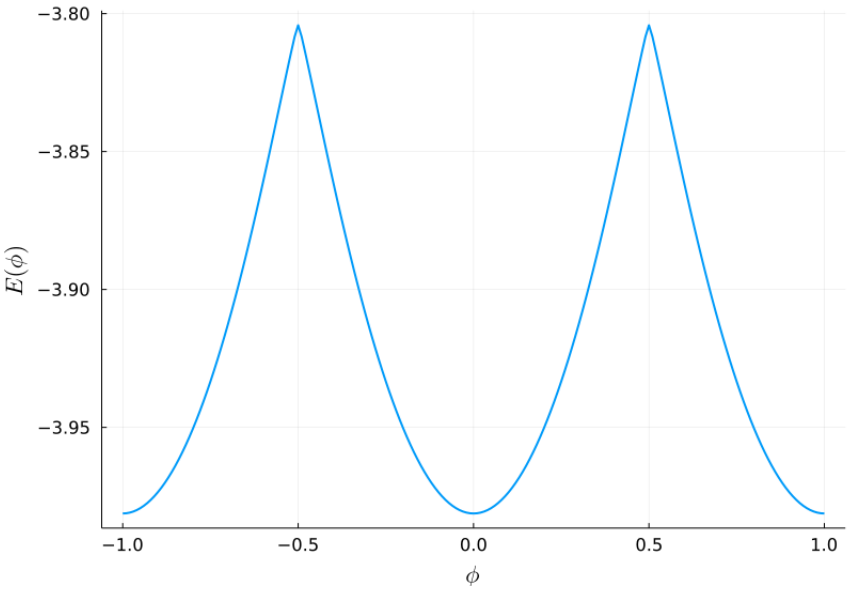


Figure 6.5: The dependence of the total energy with $\phi = \theta/2\pi$

The main result here is that the method for obtaining correlation function by means of applying the Hellman-Feynman theorem to the Galitskii-Migdal formula works very well with and without currents present, it even works reasonably well at the discontinuity. It is worth noting that this was only tested in the presence of two electrons, and that one should in principle try different configurations of the number of electrons and their spins.

If we look at table 6.1, where we compare the correlation function $\langle \hat{n}_{4+}\hat{n}_{5-}\rangle$ computed exactly in the ground state and via the GM formula, we see that the results agree down to the $8^{\text{th}}$ decimal place, exceeding the expected error of $\mathcal{O}(h)$.

| $\theta$ | $\langle\Psi_0\vert\, \hat{n}_{4+}\hat{n}_{5-}\,\vert\Psi_0\rangle$ | $(d/dv_{45}^{+-})E(v_{ij}^{\sigma\bar{\sigma}})$ |
|---|---|---|
| 0 | 0.00444333876596324 | 0.0044433376977792705 |
| $0.1(2\pi)$ | 0.0043605484711364455 | 0.0043605483668329725 |
| $0.2(2\pi)$ | 0.00408488336522125 | 0.004084881322086176 |
| $.3(2\pi)$ | 0.003508679478010966 | 0.0035086780147963736 |
| $.4(2\pi)$ | 0.0023371176286958936 | 0.0023371138357930477 |
| $\pi$ | 1.7677036158870474e-32 | 6.661338147750939e-10 |

Table 6.1: Table comparing the exact correlation (from E.D.) and the correlation function obtained by the GM method.

Our new way to compute static particle-particle correlation functions via derivatives of the GM total energy formula successfully applies to the case of finite systems, and also in the presence of currents. However, it is quite important to see if the method can be used for infinite system such as those encountered in quantum transport. This would allow one to compute correlation functions in the device region, and thus concurrence and entanglement as well.

A lead-device-lead system is infinite in size and aperiodic, with a total energy that is also infinite; hence a direct application of the GM formula is not possible. Instead, one could imagine a limiting procedure where the derivative of the GM formula is applied to larger and larger regions incorporating the device, to attain convergence when reaching far deep in the leads. This amounts to assuming that a slight variation of an interaction term in the central region (to perform the numerical derivative) produces a difference between a system with a given interaction and another with a slightly varied one, and that such a difference vanishes deep in the leads. Thus, in practice, the contributions coming from outside the considered region are neglected altogether.

We have numerically tested this approach, and noted that convergence is not really reached for quite large, albeit finite regions. Indeed, additional tests for finite rings showed that the value of the correlation function obtained in this way oscillates around the exact value on extending the region and that, only when the entire ring is considered in the GM formula, the value of the correlation function is always and obviously correct.

The Green's function in the leads can be shown to be expressible in terms of inbedding self-energies [42], where the latter in turn depend on the fully interacting Green's function in the device. This can be directly seen by applying a folding procedure similar to the one used to determine the embedding self-energy. If it is true that changing an interaction term in the device region produces changes that vanish very deep in the leads, one could incorporate the contribution of the entire leads by estimating analytically the aforementioned difference.

### 6.2.3 A possible non-perturbative G1-G2 scheme

Here we have investigated the plausibility of computing an exact two-particle Green's function in a subsystem and then using it to compute the self-energy in the original system. The investigation is by no means exhaustive, but rather represents a brief glimpse of what a G1G2-scheme [43] might have to offer.

We chose an interacting ring, of length $L = 8$, as the testing grounds for this idea, with the Hamiltonian in equation 6.1. We choose $\epsilon_i = 0$, $t = -1$ and $U_4 = 3$, i.e. the on-site energies are vanishing, the hopping strength between neighboring sites is $-1$ and the Hubbard interaction at site 4 has strength 3. For convenience of computation, we let the system contain 2 electrons with opposite spins. The Hilbert space then has size $\binom{8}{1}^2 = 64$.

From the Lehmann representation we can compute the exact non-interacting, $g$, and interacting one-particle, $G$, Green's functions:

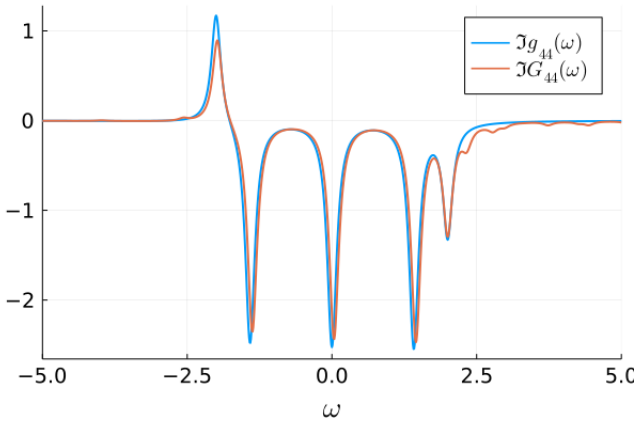


Figure 6.6: Displayed here are the non-interacting and interacting Green's function of a ring of length $L = 8$.

From $G_0$ and $G$ we can compute the exact self-energy of the system:

$$\Sigma = G_0^{-1} - G^{-1}. \tag{6.20}$$

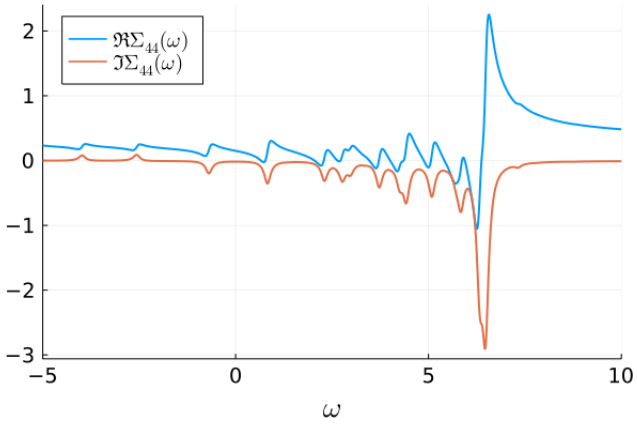


Figure 6.7: Self-energy computed by equation 3.26.

The self-energy shown in figure 6.7 is then what we will refer to here as the true self-energy of the system. As a sanity check we also show the self-energy obtained from:

$$\Sigma_{ij} = \sum_{kl} v_{ik} G_{iklk} (G^{-1})_{lj}, \tag{6.21}$$

which, with exact $G$ and $G^{(2)}$, should result in the exact self-energy as well, see figure 6.8.

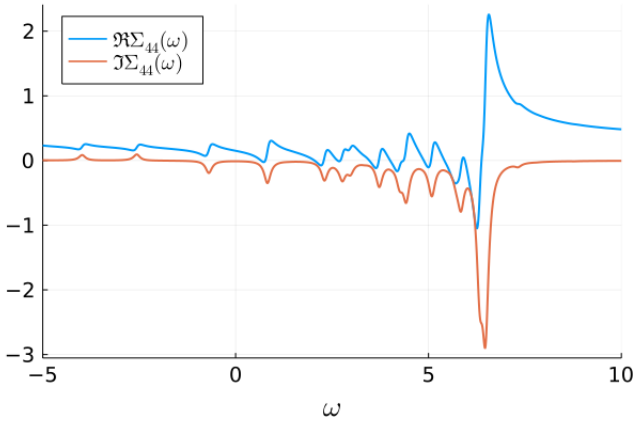


Figure 6.8: Self-energy computed by equation 3.28.

To approximate the true self-energy, we chose the subsystem to be a chain of length $L_C$ with the impurity in the center. We then test three different

lengths, $L_C$ of the subsystem, and compare the approximate self-energy in the subsystems to the true self-energy.

The Hamiltonian of the subsystem becomes:

$$\hat{H}_C = \sum_{i \in C,\sigma} \tilde{\epsilon}_{i\sigma} \hat{n}_{i\sigma} + t \sum_{<ij> \in C,\sigma} (\hat{c}^\dagger_{i\sigma} \hat{c}_{j\sigma} + \text{H.c.}) + U_4 \hat{n}_{\text{imp}+} \hat{n}_{\text{imp}-}. \tag{6.22}$$

The parameter space, $\mathcal{S}$, over which we want to minimize the norm function $f(\mathcal{S})$ in equation 6.7, we take to be that spanned by $\tilde{\epsilon}_1$ and $\tilde{\epsilon}_2$, where the former is the on-site energy of the non-interacting sites in the subsystem and the latter the on-site energy of the impurity. The hopping and interaction strength were kept true to the original system.

We used a built-in minimizer in the Julia programming language, which utilized the Nelder-Maed algorithm.

Next, we present the result for different sizes of the subsystem.

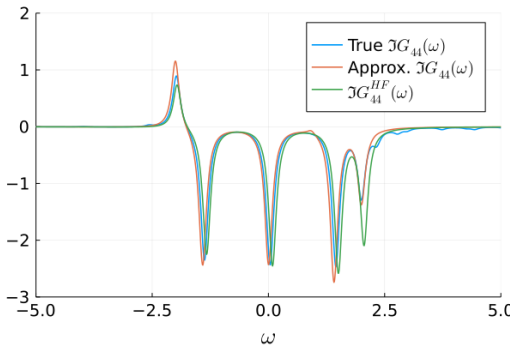


Figure 6.9: Chain of length $L_C = 3$

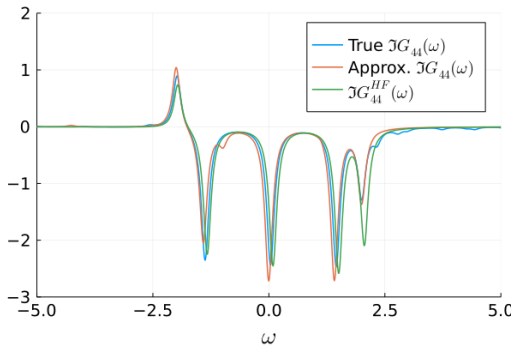


Figure 6.10: Chain of length $L_C = 5$

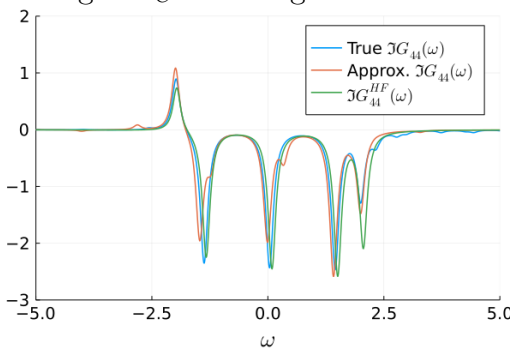


Figure 6.11: Chain of length $L_C = 7$

| $L_C$ | $\tilde{\epsilon}_1$ | $\tilde{\epsilon}_2$ | $\min(f(\mathcal{S}))$ | $\max(\lvert G^{\text{true}} - G^{\text{approx}} \rvert)$ |
|---|---|---|---|---|
| 3 | -10.413321 | 0.66882 | 5.983312 | 0.8399 |
| 5 | -4.965882 | -1.71791 | 4.339877 | 0.8388 |
| 6 | -2.420706 | -0.73211 | 2.516465 | 1.51446 |

Table 6.2: The results of minimizing $f(\mathcal{S})$ over $\{\tilde{\epsilon_1}, \tilde{\epsilon_2}\}$.

| $\epsilon_{i\neq 4}$ | $\epsilon_4$ | $\max(\lvert G^{\text{true}} - G^{\text{HF}} \rvert)$ |
|---|---|---|
| 0 | 8.90051E-02 | 0.8153 |

Table 6.3: On-site energies and deviation from exact Green's functions in the HF approximation.

We can see by visual inspection in figures 6.9-6.11 and confirmed by table 6.2 that the $L_C = 3$ and $L_C = 5$ give better approximations to the true Green's function, with the $L_C = 7$ subsystem performing significantly worse despite a producing a smaller $f(\mathcal{S})$. When comparing directly to the HF approximation, we find that the $L_C = 3$ and $L_C = 5$ are of similar accuracy. The reason for the $L_C = 7$ discrepancy could possibly be due to the norm function, $f(\mathcal{S})$, not being a particularly suitable choice for this type of optimization. Perhaps, since the carved subsystem is a chain, with open boundary conditions, and the original system a ring, a more likely reason is that the $L_C = 7$ chain may not reasonably represent a region around the impurity from the original system whereas the smaller chains might.

Our simple proposal appears to exhibit some attractive features which could prove useful in order to establish a systematic non-perturbative G1-G2 scheme. On the other hand, our analysis and conclusions rely on rather limited numerical evidence and benchmarks. More specifically; one should consider different geometries and electron configurations, and gain a more in depth understanding regarding the convergence with respect to the number of sites in the "carved" region.

# Chapter 7

# Summary & Outlook

To summarize, the non-equilibrium Green's function formalism was used to study transport geometries. The NEGF's are defined on the Keldysh contour and they encompass the other flavors of Green's function. The equation of motion of the one-particle Green's function which depends on higher order Green's functions. This leads to the introduction of the self-energy, the quantity describing particle-particle interactions. Two different levels of approximation for the self-energy were treated, HF and 2B. We briefly discussed the Feynman diagram technique of perturbatively expanding the self-energy in powers of the interaction. Ultimately the goal was to use the Green's functions in steady state, where we show that the equation of motion and the Green's function can be written in a simplified form.
We considered two different systems; an open tight-binding chain and a tight-binding ring. Open systems are in principle infinite, which obviously is unfeasible to work with, thus an embedding self-energy approach was used. The embedding energy maps the effect of the leads on to a finite region allowing one to work with a "central" region along with embedding self-energies. The finite ring was used as a testing grounds for two theoretical methods; a method for calculating two-body correlation functions and a non-perturbative G1-G2 scheme.

We found that applying the Hellman-Feynman theorem to the Galitskii-Migdal formula for the total energy, allows one to find any two-body correlation function. This prescription was tested by applying it to quantum ring geometries, where comparison with exact benchmarks showed that our method works very well both in the equilibrium regime and in the presence of steady state currents. Based on these results, and the mathematical na-

ture of the procedure involved., it is our guess that our prescription should also work well for transient currents for finite geometries (e.g. in rings or for AC fields). Applying this method to open systems should in principle also work; however, we found that a direct numerical implementation of our protocol to a lead-device-lead setup (but where contributions far deep in the leads were neglected) fails to reproduce the correct correlation function. We thus concluded that an accurate (and largely analytical) inclusion of the asymptotic contributions from the lead is a necessary ingredient to properly assess the scope of the method and, if viable, to implement it numerically.

A preliminary investigation was performed into a possible non-perturbative G1-G2 scheme. We investigate whether an exact two-particle Green's function computed in a subsystem can to any degree approximate the two-particle Green's function of the full system. We applied this method to a ring of 8 sites, with one impurity where subsystem was chosen to be a chain "cut out" of the ring.

Despite being a short investigation, we find promising results in a finite geometry. We expect better agreement between the approximate Green's function and the exact Green's function if one were to expand the parameter space $\mathcal{S}$ over which one optimizes the $f(\mathcal{S})$. Furthermore, we are currently developing a protocol to carry to this approximation in open geometries, where access to the exact Green's function is not available.

# Bibliography


[1] Nicolas Bergmann and Michael Galperin. A green's function perspective on the nonequilibrium thermodynamics of open quantum systems strongly coupled to baths: Nonequilibrium quantum thermodynamics. The European Physical Journal Special Topics, 230, 04 2021.

[2] K. Krieger, J. Dewhurst, Peter Elliott, and E.K.U. Gross. Laser-induced demagnetization at ultrashort time scales: Predictions of tddft. Journal of Chemical Theory and Computation, 11:150901135341006, 09 2015.

[3] Tobias Dornheim, Simon Groth, and Michael Bonitz. The uniform electron gas at warm dense matter conditions. Physics Reports, 744:1–86, 2018.

[4] Emil Viñas Boström, Anders Mikkelsen, Claudio Verdozzi, Enrico Perfetto, and Gianluca Stefanucci. Charge separation in donor-c60 complexes with real-time green functions: The importance of nonlocal correlations. Nano letters, 18 2:785–792, 2018.

[5] Emil Viñas Boström and Claudio Verdozzi. Steering magnetic skyrmions with currents: A nonequilibrium green's functions approach. physica status solidi (b), 256(7):1800590, 2019.

[6] J. Bardeen, L. N. Cooper, and J. R. Schrieffer. Theory of Superconductivity. Physical Review, 108(5):1175–1204, December 1957.

[7] Mingyang Guo and Tilman Pfau. A new state of matter of quantum droplets. Frontiers of Physics, 16(3):1–4, 2021.

[8] Harold Weinstock. Applications of Superconductivity. Springer, Dordrecht, 2000.

[9] Johannes Handsteiner, Andrew S. Friedman, Dominik Rauch, Jason Gallicchio, Bo Liu, Hannes Hosp, Johannes Kofler, David Bricher,

Matthias Fink, Calvin Leung, and et al. Cosmic bell test: Measurement settings from milky way stars. Physical Review Letters, 118(6), Feb 2017.

[10] Roman Schmied, Jean-Daniel Bancal, Baptiste Allard, Matteo Fadel, Valerio Scarani, Philipp Treutlein, and Nicolas Sangouard. Bell correlations in a bose-einstein condensate. Science, 352(6284):441–444, Apr 2016.

[11] Stuart J. Freedman and John F. Clauser. Experimental Test of Local Hidden-Variable Theories. prl, 28(14):938–941, apr 1972.

[12] Michael A. Nielsen and Isaac L. Chuang. Quantum Computation and Quantum Information: 10th Anniversary Edition. Cambridge University Press, 2010.

[13] Carla Figueira de Morisson Faria and X. Liu. Electron-electron correlation in strong laser fields. Journal of Modern Optics - J MOD OPTIC, 58:1076–1131, 07 2011.

[14] Jan-Philip Joost, Niclas Schlünzen, and Michael Bonitz. Femtosecond electron dynamics in graphene nanoribbons - a nonequilibrium green functions approach within an extended hubbard model. physica status solidi (b), 256:1800498, 01 2019.

[15] Nicklas Ohlsson, R Krishna Mohan, and Stefan Kröll. Quantum computer hardware based on rare-earth-ion-doped inorganic crystals. Optics Communications, 201(1):71–77, 2002.

[16] R.M. Dreizler and E.K.U. Gross. Density Functional Theory: An Approach to the Quantum Many-Body Problem. Springer Berlin Heidelberg, 2012.

[17] Antoine Georges, Gabriel Kotliar, Werner Krauth, and Marcelo J. Rozenberg. Dynamical mean-field theory of strongly correlated fermion systems and the limit of infinite dimensions. Rev. Mod. Phys., 68:13–125, Jan 1996.

[18] Miroslav Hopjan and C Verdozzi. Probing strongly correlated materials in non-equilibrium: Basic concepts and possible future trends in first principle approaches. Topics in current chemistry, 347, 05 2014.

[19] Elias Nyholm. Entanglement production in a quantum heat engine, 2020. Student Paper.

[20] Marc Friesen, C. Verdozzi, and Carl-Olof Almbladh. Can we always get the entanglement entropy from the kadanoff-baym equations? the case of the t-matrix approximation. Europhysics Letters (epl), 95, 03 2011.

[21] Peter Samuelsson and Claudio Verdozzi. Two-particle spin entanglement in magnetic anderson nanoclusters. Phys. Rev. B, 75:132405, Apr 2007.

[22] Alexander Weiße and Holger Fehske. Exact Diagonalization Techniques, pages 529–544. Springer Berlin Heidelberg, Berlin, Heidelberg, 2008.

[23] J. J. Sakurai and Jim Napolitano. Modern Quantum Mechanics. Cambridge University Press, 3 edition, 2020.

[24] Philip Johansson. Real-time entanglement of auger and xps-electrons: a preliminary investigation, 2019. Student Paper.

[25] Leonid Keldysh. Diagram technique for nonequilibrium processes. Soviet Physics JETP, 1965.

[26] Gianluca Stefanucci and Robert van Leeuwen. Nonequilibrium Many-Body Theory of Quantum Systems: A Modern Introduction. Cambridge University Press, 2013.

[27] David C. Langreth. Linear and Nonlinear Response Theory with Applications. Springer US, Boston, MA, 1976.

[28] M J Hyrkäs, D Karlsson, and R van Leeuwen. Contour calculus for many-particle functions. Journal of Physics A: Mathematical and Theoretical, 52(21):215303, apr 2019.

[29] Anna-Maija Uimonen. Many-body approach to time-dependent quantum transport. PhD thesis, 01 2009.

[30] Harry Lehmann. Über eigenschaften von ausbreitungsfunktionen und renormierungskonstanten quantisierter felder. Il Nuovo Cimento (1943-1954), 11(4):342–357, 1954.

[31] V. M. Galitskii and A. B. Migdal. 7(96), 1958.

[32] Y Meir and NS Wingreen. Landauer formula for the current through an interacting electron region. Physical review letters, 68(16):2512 – 2515, 1992.

[33] R.D. Mattuck. A Guide to Feynman Diagrams in the Many-body Problem. Dover Books on Physics Series. Dover Publications, 1992.

[34] F Aryasetiawan and O Gunnarsson. TheGWmethod. Reports on Progress in Physics, 61(3):237–312, mar 1998.

[35] N Schlünzen, S Hermanns, M Scharnke, and M Bonitz. Ultrafast dynamics of strongly correlated fermions—nonequilibrium green functions and selfenergy approximations. Journal of Physics: Condensed Matter, 32(10):103001, dec 2019.

[36] Fftw home page , `https://www.fftw.org/`.

[37] J. A. Nelder and R. Mead. A Simplex Method for Function Minimization. The Computer Journal, 7(4):308–313, 01 1965.

[38] A.-M. Uimonen, E. Khosravi, G. Stefanucci, S. Kurth, R. van Leeuwen, and E.K.U. Gross. Real-time switching between multiple steady-states in quantum transport. 220(1):012018, 2010.

[39] Karlsson Daniel and Verdozzi Claudio. Effective bias and potentials in steady-state quantum transport: A negf reverse-engineering study. Journal of Physics: Conference Series, 696(1):1, 2016.

[40] Madhumita Saha and Santanu Maiti. Circulating current in 1d hubbard rings with long-range hopping: Comparison of exact diagonalization method and mean-field approach. Physica E: Low-dimensional Systems and Nanostructures, 84, 03 2016.

[41] HF Cheung, EK Riedel, and Y Gefen. Persistent currents in mesoscopic rings and cylinders. Physical review letters, 62(5):587 – 590, 1989.

[42] Petri Myöhänen, Adrian Stan, Gianluca Stefanucci, and Robert van Leeuwen. Kadanoff-Baym approach to time-dependent quantum transport in AC and DC fields. In Journal of Physics Conference Series, volume 220 of Journal of Physics Conference Series, page 012017, April 2010.

[43] Niclas Schlünzen, Jan-Philip Joost, and Michael Bonitz. Achieving the scaling limit for nonequilibrium green functions simulations. Physical Review Letters, 124, 02 2020.